Conditional immortalization of human atrial myocytes for the generation of in vitro models of atrial fibrillation

Harlaar, N.; Dekker, S.O.; Zhang, J.; Snabel, R.R.; Veldkamp, M.W.; Verkerk, A.O.; ... ; Vries, A.A.F. de

nature biomedical engineering

ARTICLES

https://doi.org/10.1038/s41551-021-00827-5

Check for updates

Conditional immortalization of human atrial myocytes for the generation of in vitro models of atrial fibrillation

Niels Harlaar[1,2], Sven O. Dekker[1], Juan Zhang[1], Rebecca R. Snabel[3], Marieke W. Veldkamp[4], Arie O. Verkerk[4,5], Carla Cofiño Fabres[6], Verena Schwach[6], Lente J. S. Lerink[1], Mathilde R. Rivaud[4], Aat A. Mulder[7], Willem E. Corver[8], Marie José T. H. Goumans[7], Dobromir Dobrev[9], Robert J. M. Klautz[2], Martin J. Schalij[1], Gert Jan C. Veenstra[3], Robert Passier[6], Thomas J. van Brakel[2], Daniël A. Pijnappels[1,10] and Antoine A. F. de Vries[1,10] ✉

The lack of a scalable and robust source of well-differentiated human atrial myocytes constrains the development of in vitro models of atrial fibrillation (AF). Here we show that fully functional atrial myocytes can be generated and expanded one-quadrillion-fold via a conditional cell-immortalization method relying on lentiviral vectors and the doxycycline-controlled expression of a recombinant viral oncogene in human foetal atrial myocytes, and that the immortalized cells can be used to generate in vitro models of AF. The method generated 15 monoclonal cell lines with molecular, cellular and electrophysiological properties resembling those of primary atrial myocytes. Multicellular in vitro models of AF generated using the immortalized atrial myocytes displayed fibrillatory activity (with activation frequencies of 6–8 Hz, consistent with the clinical manifestation of AF), which could be terminated by the administration of clinically approved antiarrhythmic drugs. The conditional cell-immortalization method could be used to generate functional cell lines from other human parenchymal cells, for the development of in vitro models of human disease.

Preclinical biomedical research across academia and industry strongly relies on in vitro models to advance pathophysiological knowledge and to develop novel therapeutics. Human disease models based on (cultured) animal cells are becoming less popular owing to the growing awareness of the existence of principal differences in (patho)physiology between humans and animals and to the increasing public opposition to animal testing[1]. This has created a large demand for difficult-to-obtain human parenchymal cells, including cardiomyocytes, hepatocytes and neurons. Acquisition of such terminally differentiated cell types is complicated by the fluctuating availability and inconsistent quality of source material including post-mortem samples, surgical waste, non-transplanted donor tissue and biopsies. Additionally, these cell types cannot be multiplied in vitro and rapidly dedifferentiate in culture, severely restricting the window of use after isolation. Also, permanent human cell lines of tumour origin or created through genetic engineering generally have not been able to recapitulate the functional properties of the primary cells from which they were derived, because continuing proliferation inhibits differentiation in most cell types[2].

Many of these drawbacks have been overcome by the establishment of human embryonic stem cell (hESC) lines[3] and, more recently, of human induced pluripotent stem cell (hiPSC) lines[4,5], in conjunction with the development of new methods to derive various differentiated cell types from them. As a result, human (pluripotent) stem cell-based two-dimensional and three-dimensional multicellular in vitro models including organoids[6] are rapidly gaining popularity for human-disease modelling, target identification, drug development and therapeutic testing. A particularly attractive feature of hiPSCs is the ease with which they can be generated from individual patients, allowing the development of patient-specific disease models, thereby creating unique opportunities for personalized medicine. Despite the many advantages of human (pluripotent) stem cell-based in vitro models, there are still several factors that limit their application: first, the derivation of specialized cells from human (pluripotent) stem cells is often a complex and laborious process with variable outcomes; second, producing large numbers of specialized cells with a high degree of phenotypic uniformity from human (pluripotent) stem cells is difficult; and third, the differentiated progeny of human (pluripotent) stem cells typically has an immature phenotype and thus functionally differs from adult human cells.

In an attempt to address these limitations, we recently developed a monopartite lentiviral vector (LV)-based system for the conditional immortalization of primary mammalian cells[7,8]. At the heart of this system is a recombinant simian virus 40 (SV40) large T (LT)

[1]Department of Cardiology, Leiden University Medical Center, Leiden, the Netherlands. [2]Department of Cardiothoracic Surgery, Leiden University Medical Center, Leiden, the Netherlands. [3]Department of Molecular Developmental Biology, Radboud University, Nijmegen, the Netherlands. [4]Department of Clinical and Experimental Cardiology, Amsterdam UMC, Amsterdam, the Netherlands. [5]Department of Medical Biology, Amsterdam UMC, Amsterdam, the Netherlands. [6]Applied Stem Cell Technologies, University of Twente, Enschede, the Netherlands. [7]Department of Cell and Chemical Biology, Leiden University Medical Center, Leiden, the Netherlands. [8]Department of Pathology, Leiden University Medical Center, Leiden, the Netherlands. [9]Institute of Pharmacology, University Duisburg-Essen, Essen, Germany. [10]These authors contributed equally: Daniël A. Pijnappels, Antoine A.F. de Vries. ✉e-mail: a.a.f.de_vries@lumc.nl

gene, the expression of which is driven by a cell type-specific promoter and can be repeatedly switched on and off by means of the tetracycline/doxycycline (dox)-controlled transcription silencer TetR-KRAB[9,10]. Here we employ this conditional-immortalization method to generate lines of human atrial myocytes (AMs) with preserved cardiomyogenic differentiation capacity. The reasons for choosing human AMs as target cells are two-fold: their highly specialized nature and specific functional properties (that is, excitability and contractility) provide a stringent test for the effectiveness of our conditional cell-immortalization system; and the rapid worldwide increase in the prevalence of atrial fibrillation (AF)[11], its high socioeconomic burden[12], incomplete mechanistic understanding[13], substantial translational challenges[14] and suboptimal treatment options[15] have created an urgent need for a robust source of human AMs to overcome the current lack of clinically relevant (in vitro) models of AF[16].

Transduction of human foetal AMs (hfAMs) with the TetR-KRAB-regulated LT-encoding LV resulted in the generation of 15 monoclonal cell lines, designated hiAMs, that rapidly proliferated in the presence of dox and differentiated into excitable and contractile cells with molecular, cellular and electrophysiological properties of AMs after dox withdrawal. These cell lines were used to establish multicellular in vitro AF models featuring fibrillatory activity with clinically relevant dynamics and activation frequencies, which could be terminated with traditional antiarrhythmic drugs. The development of the hiAM lines provides proof-of-concept of a versatile method to produce, in a simple and rapid manner, massive numbers of authentic human cells for comprehensive disease modelling.

Results

Generation and selection of hiAMs. To conditionally immortalize human atrial cardiomyocytes, human foetal atrial tissue (gestational age, 18 weeks) was dissociated. The resulting cell suspension was transduced with LV particles containing a dox-inducible SV40 LT expression unit driven by the strong hybrid striated muscle-specific MHCK7 promoter[17], targeting the cardiomyocyte population in the atrial cell mixture (Fig. 1a and Supplementary Fig. 1). Two to three weeks after induction of SV40 LT synthesis through addition of dox and reseeding cells at ultralow density, proliferating colonies comprising 100–200 cells appeared (Fig. 1b). To assess whether the conditional immortalization was successful, 95 proliferating colonies were isolated, expanded and graded using predefined criteria to assess both the proliferative activity of the cells in the presence of dox and their ability to reacquire the differentiated properties of AMs following dox removal (Fig. 1c and Supplementary Fig. 1). To meet these criteria, the monoclones should display the following properties: (1) proliferate well in the presence of dox (>15 population doublings (PDs) with a doubling time <120 h), (2) cease proliferation following dox removal and acquire a cardiomyocyte-like phase-contrast appearance after 12 days of culture in differentiation medium, (3) stain negative for proliferation marker Ki-67 and positive for cardiac troponin T (TNNT2) at 12 days after dox withdrawal and (4) generate and conduct (typical atrial) electrical impulses following cardiomyogenic differentiation in confluent monolayers (action potential (AP) duration (APD) at 80% repolarization (APD_{80}) < 300 ms and conduction velocity (CV) > 10 cm s^{-1}) (Fig. 1d,e and Supplementary Fig. 1). Fifteen of the 95 (15.8%) monoclones, designated human immortalized AMs (hiAMs), adhered to all 4 predefined criteria indicating successful generation, through conditional immortalization, of human cardiomyocyte lines with preserved cardiomyogenic differentiation capacity.

Characterization of hiAMs during proliferation and after differentiation. Three of the 15 hiAM clones (clones 2.38, 2.52 and 2.90) were randomly selected for in-depth characterization (Fig. 1f). The number of lentiviral integrations in these clones ranged from 4 to 6 (Supplementary Table 1). Analysis of their DNA content revealed all 3 clones to comprise predominantly cells with DNA indices between 1.7 and 1.8 (Supplementary Fig. 2 and Table 2). The doubling time of the 3 selected hiAM clones in the presence of dox was 55 ± 5 h (Fig. 1g). Proliferating hiAMs contained a much higher percentage of Ki-67$^+$ nuclei than freshly isolated hfAMs (Fig. 1h). The low Ki-67 expression in hfAMs is consistent with the limited mitotic activity of human cardiomyocytes in the second semester of gestation[18]. hiAMs could be expanded for at least 50 PDs without a noticeable reduction in proliferation rate, resulting in ≥quadrillion-fold cell multiplication. Dox omission in the culture medium resulted in a strong (>2,000-fold) reduction of the SV40 LT level in hiAMs over the course of 12 d, as determined by western blotting (Fig. 1i). At the same time, hiAMs no longer displayed any Ki-67$^+$ nuclei.

The 12 day transition from a proliferating to a differentiated hiAM, which is simply initiated by the removal of dox and a change from proliferation to differentiation medium, was accompanied by the reappearance of spontaneous synchronous contractions similar to those observed in freshly isolated hfAMs (Supplementary Video 1). Immunostaining for the sarcomeric proteins α-actinin 2 (ACTN2), TNNT2 and the atrial isoform of myosin regulatory light chain 2 (MLC2a), showed that the highly organized sarcomeres observed in hfAMs were lost following conditional immortalization and induction of proliferation, but reappeared when hiAMs were growth-arrested by dox withdrawal and allowed to redifferentiate for 12 days (Fig. 2a and Supplementary Fig. 3). Flow cytometric analysis showed that hiAM differentiation yielded highly pure cell populations, comprising on average 99.1% ACTN2-positive and 97.2% TNNT2-positive cells (Supplementary Fig. 4). Gap junctional protein connexin-43, which was concentrated at cell–cell interfaces in hfAMs, also disappeared when proliferation was induced and again formed neatly organized cell–cell connections following hiAM differentiation (Fig. 2a). Additionally, hiAM differentiation caused an increase in the levels of the atrium-specific gap junctional protein connexin-40 (Supplementary Fig. 3). Detailed imaging by transmission electron microscopy revealed the presence of well-organized sarcomeres, perinuclear and intermyofibrillar mitochondria, and intercalated discs in differentiated hiAMs (Supplementary Fig. 5). Sarcomere lengths appeared to be slightly shorter in differentiated hiAMs (1.79–1.83 µm) compared with hfAMs (1.96 µm, Supplementary Fig. 3). At all stages, hfAMs and hiAMs stained negative for the ventricular isoform of myosin regulatory light chain 2 (MLC2v), corroborating their atrial origin and specificity.

We next performed RNA sequencing to study the transcriptome of proliferating and cardiomyogenically differentiated hiAMs (Fig. 2b). Principal component analysis and heatmaps of global gene expression data illustrated a clear separation between the transcriptomes of the proliferating (D0) and differentiated (D12) hiAM clones (Fig. 2c). Grouped comparison revealed 6,078 differentially expressed genes (DEGs), of which 2,652 were downregulated and 3,426 were upregulated when transitioning from proliferation to differentiation (log_2 fold change >1 and false discovery rate (FDR)-corrected $P < 0.001$, Supplementary Data File 1). Differential gene expression of individual clones showed a large overlap (Fig. 2d). Downregulated genes standing out (including MKI67, AURKB, CDK1, CCNA2 and POLE) appeared to be closely involved with cell proliferation, whereas upregulated genes (such as ACTN2, MYH6, KCNJ2, CACNA1C and GJA5) were associated with a differentiated AM phenotype (Fig. 2e). These observations were confirmed by gene ontology (GO) analysis of the up- and down-regulated genes (Fig. 2f and Supplementary Fig. 6). GO terms enriched during hiAM proliferation were mainly related to DNA replication and cell division, whereas the most enriched GO terms post differentiation were involved in myofibrillogenesis,

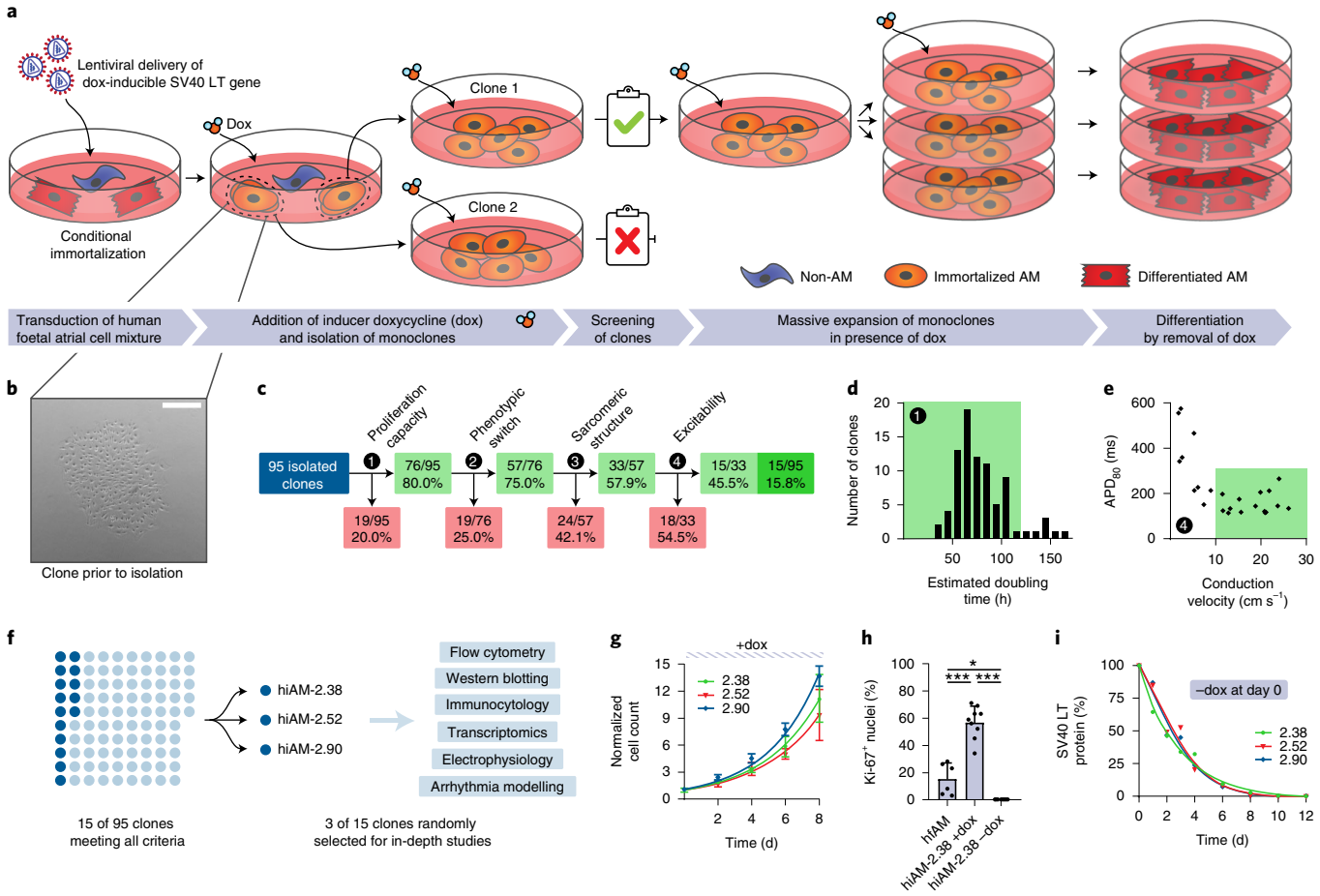

Fig. 1 | Generation and selection of hiAM monoclones. a, Schematic overview of the conditional immortalization of hfAMs, generation and selection of hiAM monoclones, massive hiAM expansion in the presence of dox and cardiomyogenic differentiation of hiAMs following dox removal. **b**, Representative phase-contrast image of a hiAM monoclone before isolation. Scale bar, 500 µm. **c**, Flowchart of hiAM monoclone selection based on 4 main criteria (labelled 1 to 4), with corresponding drop-off rates (see Supplementary Fig. 1 for additional data). **d**, Estimated doubling time of isolated hiAM monoclones based on passaging intervals. The highlighted area (doubling time ≤120 h) represents a pass on the first selection criterion. **e**, Selection based on excitability of hiAM monoclones using optical voltage mapping as part of the fourth selection criterion. The highlighted area represents selected monoclones with a CV ≥ 10 cm s^{-1} and APD_{80} ≤ 300 ms. **f**, Summary of monoclone selection. hiAM clones 2.38, 2.52 and 2.90 were selected for further characterization. **g**, Quantification of hiAM proliferation in the presence of dox ($n = 3$ independent experiments per monoclone; mean ± s.d.). **h**, Ki-67$^+$ nuclei determined by immunocytochemistry in hfAM ($n = 2$), proliferating (+dox, $n = 3$) hiAM and differentiated (−dox, $n = 3$) hiAM cultures. Three random areas per culture were selected for quantification. *n* signifies independent samples/differentiations. Mean ± s.d.; $^*P < 0.05$, $^{***}P < 0.001$, one-way ANOVA with Tukey post-hoc analysis. **i**, SV40 LT levels in proliferating hiAM-2.38, -2.52 and -2.90, measured by western blotting over 12 days of differentiation following removal of dox at day 0 ($n = 1$ per monoclone).

energy metabolism and cardiac muscle contraction. The differential expression levels of atrial and ventricular marker genes, such as MYL7/MYL2 (19,669.6 vs 0.2 transcripts per million (TPM)) and MYH6/MYH7 (1,126.4 vs 15.6 TPM), as well as the high abundance of NPPA transcripts (8,494.6 TPM), further confirmed the atrial phenotype of differentiated hiAMs (Supplementary Fig. 7). Collectively, these results demonstrate that the conditional immortalization by TetR-KRAB-regulated SV40 LT gene expression allows hfAMs to effectively switch between proliferative and differentiated states, which could not be achieved with permanent immortalization (Supplementary Fig. 8).

Maturity of the differentiated hiAM transcriptome. Benchmarking of hiAM maturity was first performed by comparison of the global hiAM transcriptome against compendia of gene expression data from human foetal cardiac tissues[19] and human adult tissues[20]. For reference purposes, the transcriptomic maturity of hESC-derived atrial cardiomyocytes (hESC-AMs) was also determined. The transcription profiles of hESC-AMs and differentiated hiAMs best correlated with those of atrial myocardium. However, the transcriptome of hESC-AMs correlated modestly better with that of foetal atrial myocardium, whereas the gene expression profile of hiAMs was somewhat closer to that of adult atrial myocardium (Fig. 3a).

Differential gene expression analysis between hESC-AMs and hiAMs revealed 2,276 DEGs upregulated in hESC-AMs and 1,869 DEGs upregulated in hiAMs (Fig. 3b). Neither of the gene sets was exclusively expressed in the heart, but overall, the DEGs upregulated in hiAMs were more abundantly expressed (Fig. 3c). Clustering analysis revealed that a subset of the upregulated DEGs had striated muscle-specific expression, which included SCN5A, CASQ2 and SLN for hiAMs, and MYL2, TTN and RYR2 for hESC-AMs (Supplementary Fig. 9 and Data File 2). Finally, rank-based comparison of selected maturity-related gene sets in hiAMs, hESC-AMs, foetal atrial myocardium and adult atrial myocardium revealed differences in structural, electrophysiological, contractile and metabolic properties (full overview in Supplementary Fig. 10). Overall,

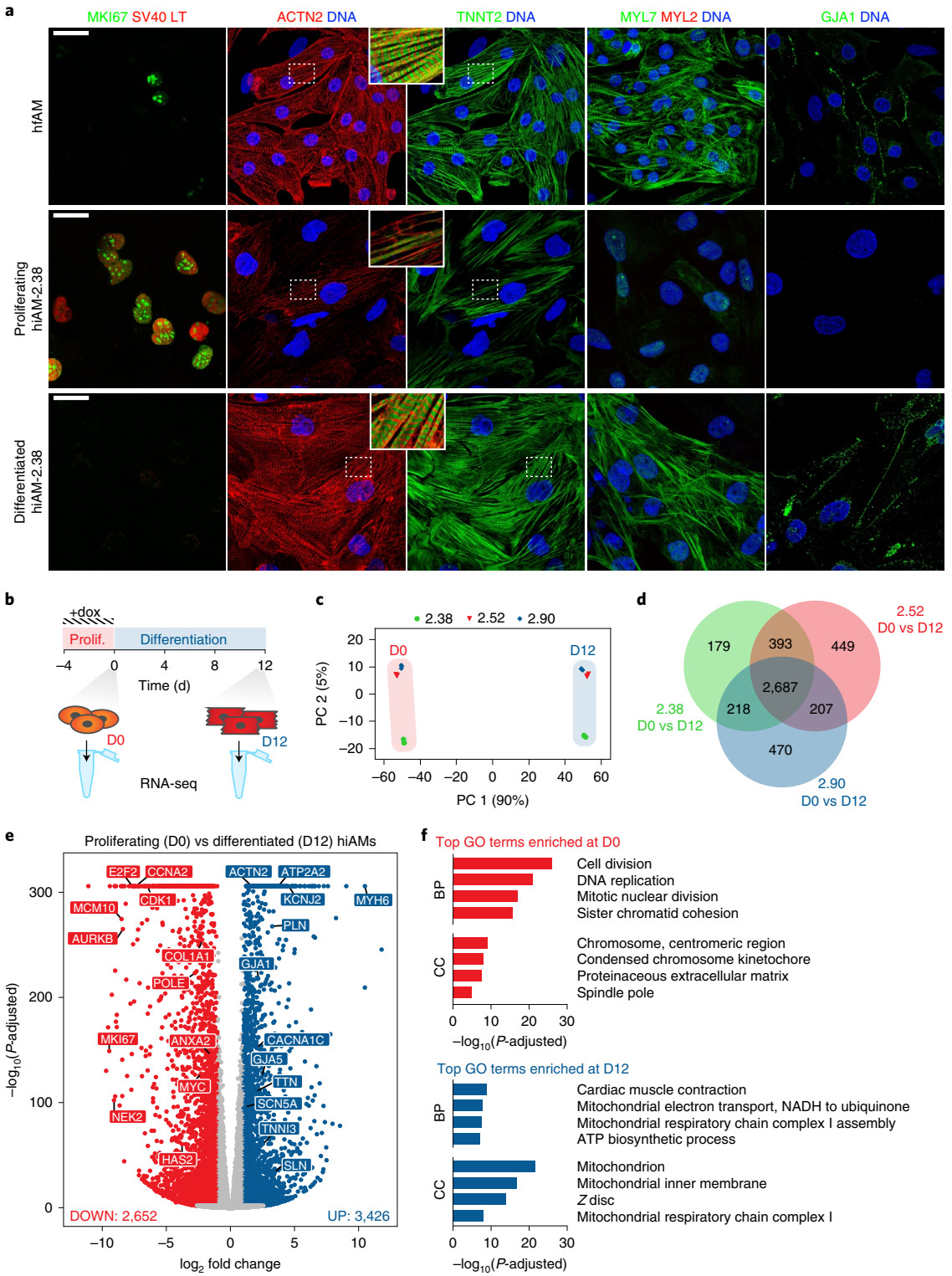

Fig. 2 | Characterization of the hiAM phenotype during proliferation and after 12 days of differentiation. a, Immunostaining of hfAMs and of proliferating and differentiated hiAM-2.38 for Ki-67 (MKI67), SV40 LT, α-actinin 2 (ACTN2), cardiac muscle troponin T (TNNT2), the atrial and ventricular isoforms of myosin regulatory light chain 2 (MYL7 and MYL2, respectively) and connexin-43 (GJA1). Dashed lines demarcate the magnified areas shown in the insets. Scale bar, 25 μm. **b**, Schematic representation of sample collection timeline for RNA sequencing. **c**, Principal component (PC) analysis of global gene expression data ($n = 3$ biological replicates per time point and hiAM clone). **d**, Venn diagram of DEGs between proliferating (D0) and differentiated (D12) hiAM-2.38, -2.52 and -2.90. Genes with >1 TPM at D0 or D12, an absolute $\log_2$ fold change >1 and an FDR-corrected $P < 0.001$ are shown. **e**, Volcano plot of gene expression in proliferating vs differentiated hiAMs (grouped analysis of hiAM clones 2.38, 2.52 and 2.90). Selected genes of interest are labelled. Please note that due to filtering applied in the comparison of the individual clones, the number of DEGs is lower than in the grouped analysis. **f**, Top four biological process (BP) and cellular component (CC) GO terms enriched in proliferating (D0) and differentiated (D12) hiAMs (see Supplementary Fig. 6 for all enriched GO terms).

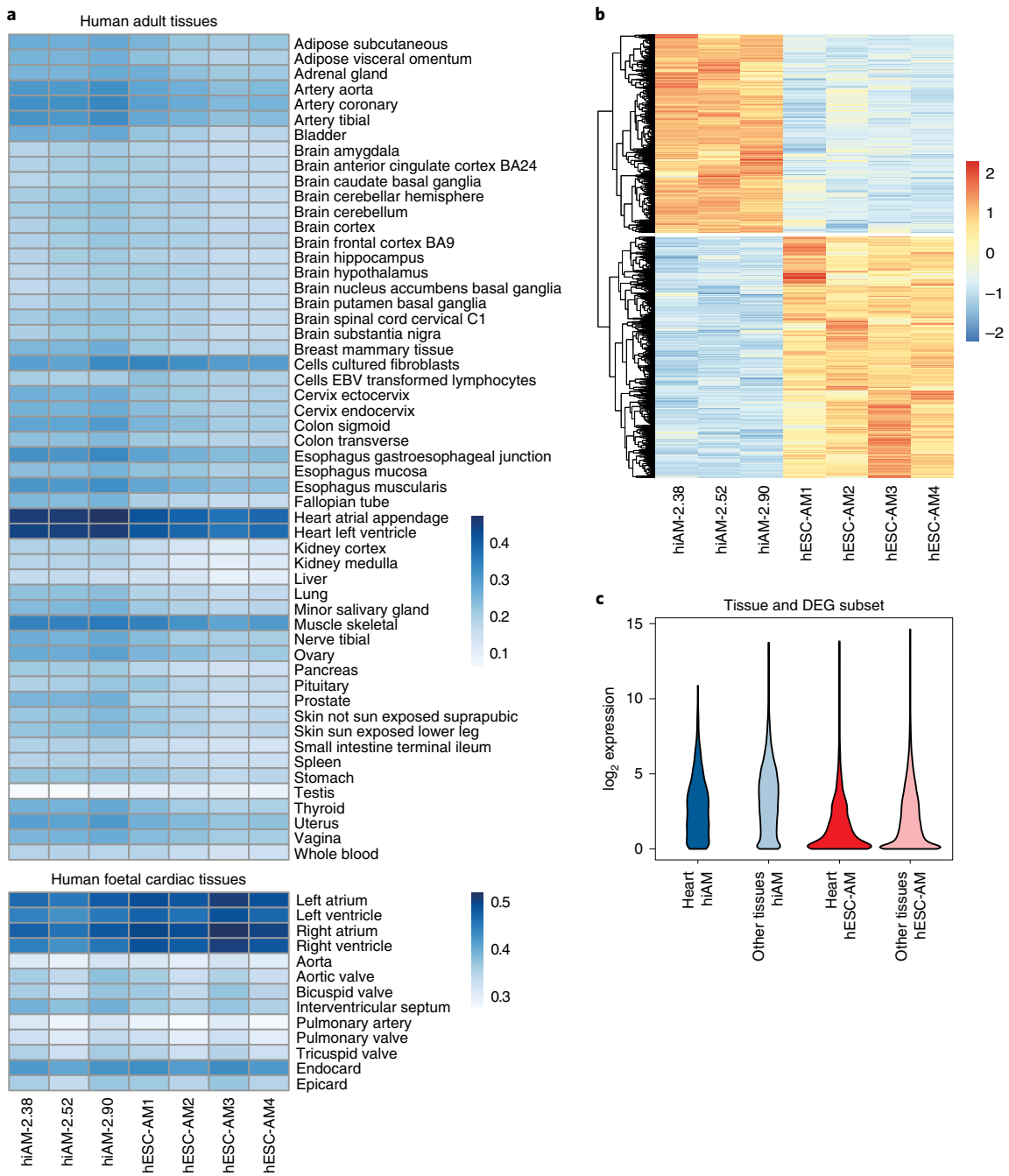

Fig. 3 | Characterization of differentiated hiAM and hESC-AM transcriptomes. a, Global transcriptome comparison of 3 hiAM clones (hiAM-2.38, -2.52 and -2.90) and of 4 hESC-AM replicates against a compendium of human adult tissues and human foetal cardiac tissues. Scale bar indicates Spearman correlation. **b**, Differential gene expression between hiAMs and hESC-AMs. Scale bar indicates row-scaled and centred expression values. **c**, Expression levels of DEGs separated on the basis of hiAM or hESC-AM specificity and cardiac or non-cardiac specificity.

these data indicate that the gene expression profile of differentiated hiAMs possesses many features of the adult atrial myocardial transcriptome.

Electrophysiological properties of differentiated hiAMs. The electrophysiological properties of cardiomyogenically differentiated hiAMs were first studied by single-cell patch-clamp analysis. Differentiated hiAM-2.38 had a resting membrane potential (RMP) similar to that of human adult AMs (haAMs) and significantly more negative than the RMP of hfAMs (Fig. 4a,b). Additionally, the maximal AP amplitude in hiAM-2.38 was larger than in hfAMs but smaller than in haAMs, whereas the AP plateau amplitude was higher in hiAM-2.38 compared with both hfAMs and haAMs. The maximum AP upstroke velocity of hiAM-2.38 was between that of hfAMs and haAMs. APD at 20, 50 and 90% of repolarization did not significantly differ between hfAMs, hiAM-2.38 and haAMs. AP characteristics similar to hiAM-2.38 were also observed in differentiated hiAM-2.52 and hiAM-2.90 (Supplementary Fig. 11 and Table 3). Subsequent voltage-clamp recordings in hiAM-2.38 showed the presence of a strong Na^+ current (I_{Na}) and robust steady-state K^+ currents (Supplementary Fig. 12), which were consistent with the fast upstroke velocity and haAM-like RMP of hiAM-2.38,

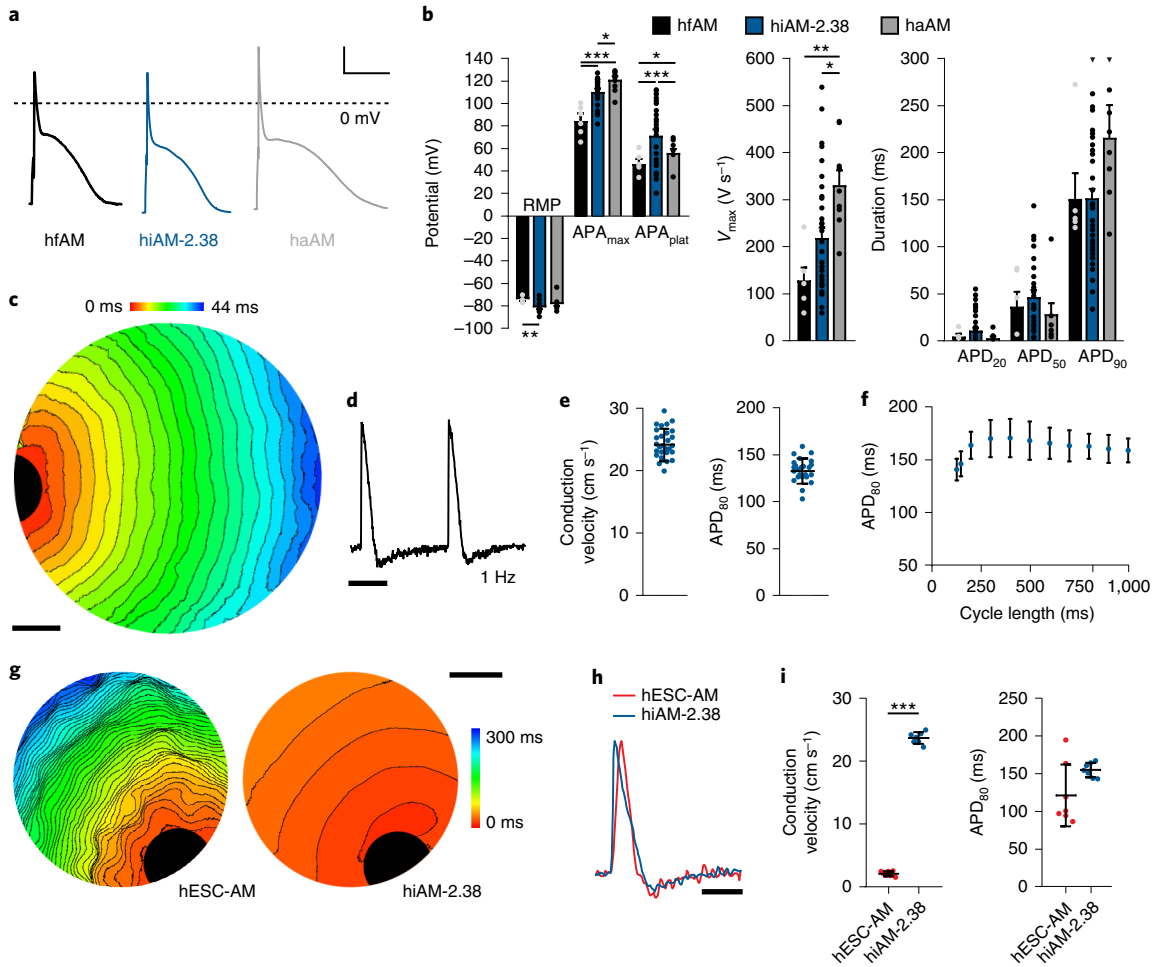

Fig. 4 | Electrophysiological characteristics of differentiated hiAMs. a,**b**, Representative AP traces (**a**) and mean AP parameters (**b**) of single hfAMs ($n=6$ cells from 2 independent preparations), single differentiated hiAM-2.38 ($n=39$ cells from 11 independent differentiations) and single haAMs ($n=9$ cells) during 1 Hz electrical stimulation. APA_{max}, maximal AP amplitude. APA_{plat}, AP plateau amplitude. V_{max}, maximum AP upstroke velocity. $APD_{20/50/90}$, action potential duration at 20, 50 and 90% of repolarization. Scale bars in **a**: x = 100 ms, y = 20 mV. The dotted line in **a** indicates the 0 mV level. Mean ± s.e.m.; $^{**}P<0.01$, $^{***}P<0.001$, one-way ANOVA with Tukey post-hoc analysis. **c**–**f**, Optical voltage mapping of confluent layers of differentiated hiAMs in a 24-well format following 1 Hz electrical point stimulation. **c**, Representative activation map of hiAM layer. Isochrones, 2 ms. Scale bar, 2 mm. **d**, Representative optical voltage trace of hiAMs from **c**. Scale bar, 500 ms. **e**, Mean CV and APD_{80} in confluent hiAM layers ($n=28$ layers from 8 independent differentiations). Mean ± s.d. **f**, APD restitution curve of hiAM-2.38 ($n=10$ layers from 2 independent differentiations). Mean ± s.d. **g**,**h**, Optical voltage mapping of confluent hESC-AM and differentiated hiAM-2.38 layers in a 48-well format. **g**, Representative activation maps of hESC-AM and hiAM-2.38 layers. Isochrones, 6 ms. Scale bar, 2 mm. **h**, Representative optical voltage traces from hESC-AMs and hiAMs of **g**. Scale bar, 250 ms. **i**, Mean CV and APD_{80} during 1 Hz electrical stimulation in hESC-AM ($n=7$ layers from 3 independent differentiations) and differentiated hiAM ($n=7$ layers from 2 independent differentiations) layers. Mean ± s.d.; $^{***}P<0.001$, unpaired *t*-test.

respectively. Finally, a strong atrial-selective 4-aminopyridine (50 µM)-sensitive ultrarapid delayed rectifier K^+ current (I_{Kur}) was present in hiAMs, validating their atrial electrophysiological phenotype (Supplementary Fig. 12 and Table 4). Overall, the electrophysiological properties of differentiated hiAMs strongly resemble those of primary human AMs.

Next, we assessed the conduction of APs in multicellular preparations by optical voltage mapping. Upon 1 Hz electrical point stimulation, cell layers (2 cm^2) of hiAM-2.38 displayed homogeneous conduction of APs (Fig. 4c,d), with a CV of 24.4 ± 2.3 cm s^{-1} and APD_{80} of 136 ± 12 ms (Fig. 4e), with APD restitution occurring at high activation frequencies (Fig. 4f). Optical voltage mapping of hiAM-2.52 and hiAM-2.90 also showed homogeneous conduction of APs at speeds of 19.4 ± 2.0 cm s^{-1} and 11.9 ± 2.0 cm s^{-1}, and APD_{80} of 129 ± 15 ms and 103 ± 9 ms, respectively (Supplementary Fig. 11). Since confluent monocultures of hfAMs or haAMs could not be established because of shortage of source material, difficulties in removing the large percentage of non-cardiomyocytes from the starting material, minimal cardiomyocyte proliferation and/or poor cardiomyocyte survival, we used hESC-AMs for comparison. Due to limited production capacity of phenotypically homogenous hESC-AM populations, this comparison was performed in confluent 1 cm^2 cell layers. While hESC-AM layers had a high spontaneous beating rate consistent with their immature phenotype, spontaneous activity was rarely observed in hiAM-2.38 layers, but could be induced by chronotropic stimulation (Supplementary Fig. 13). Following 1 Hz electrical point stimulation, conduction in hESC-AM layers appeared more heterogeneous and was >10-fold slower compared with hiAM-2.38 layers of the same size (Fig. 4g–i and Supplementary Video 2). In terms of optical AP characteristics, the optical upstroke time was longer in hESC-AMs compared with hiAM-2.38 (28 ± 6 vs 12 ± 1 ms, $P<0.001$, $n=6$ and 7, respectively),

while APD_{80} did not statistically differ between hESC-AMs and hiAMs. Similar differences in kinetics were found when comparing optically recorded Ca^{2+} transients between hESC-AM and hiAM-2.38 layers (Supplementary Results and Fig. 14).

Robustness of hiAM differentiation. From the perspective of standardization, we assessed the robustness of hiAM differentiation. Massive expansion of hiAMs did not jeopardize their cardiomyogenic differentiation potential. Comparison of optical voltage mapping data of hiAM-2.38 that had undergone different PDs (between 28 and 46) before cardiomyogenic differentiation, revealed no significant change in average CV or APD_{80} (Fig. 5a and Supplementary Fig. 15). Also, no variation in structural characteristics as assessed by immunostaining for ACTN2 and TNNT2 was observed over this broad range of PDs (Supplementary Fig. 15). Furthermore, repeatedly switching hiAMs back and forth between proliferation and differentiation did not noticeably alter their respective phenotypes. Specifically, the number of Ki-67$^+$ nuclei during proliferation, as well as the CV, APD_{80} and TNNT2 immunostaining pattern after differentiation were not affected by the repeated phenotypic transitions (Fig. 5b and Supplementary Fig. 16). Next, we tested whether hard-to-control variations in the culture medium, such as the variable composition of foetal bovine serum (FBS)[21], would affect cardiomyogenic differentiation. The CV of hiAM cultures differentiated with four different sources of FBS did not significantly differ (Fig. 5b). Similarly, no effect on APD_{80} was found, except that the premium FBS of USA origin had a minimal shortening effect on APD_{80} compared with the FBS from South America, New Zealand and Brazil (Fig. 5b). Finally, we investigated whether cryopreservation of differentiated hiAMs (in addition to cryopreservation of proliferating hiAMs) would be feasible. Thawing of hiAMs that had been cryopreserved at day 8 of differentiation, that is, just before they exhibit contractions, resulted in 91.9 ± 1.6% viable cells and an attachment efficiency of 70.4 ± 5.2% (Fig. 5c). Following 6 additional days of culture in supplemented differentiation medium to complete cardiomyogenesis, the hiAM layers did not show significant differences in electrophysiological characteristics when compared with control layers established with hiAMs that had not been cryopreserved in a partially differentiated state (Fig. 5d). Together, these data demonstrate robust hiAM differentiation irrespective of passage history, culture conditions or intermediate cryopreservation.

hiAMs as atrial arrhythmia model. We next investigated the suitability of hiAMs for AF modelling. As induction of reentry in hiAM layers was not feasible in the 2 cm² format and the average area of reentrant circuits in human AF is ~3 cm² (ref. [22,23]), we used 10 cm² confluent hiAM layers to provide space for multiple reentrant circuits. hESC-AM layers of 1 cm² were included for comparison because of the aforementioned difficulty in establishing larger confluent monolayers of these cells. Upon high-frequency electrical point stimulation, arrhythmic activity with varying degrees of complexity could be induced in both 1 cm² hESC-AM and 10 cm² hiAM layers (Fig. 6a,b and Supplementary Video 3). Reentrant activity induced in hESC-AM layers had an average activation frequency of 3.0 ± 0.8 Hz, which was consistent with previous reports of arrhythmic hESC-AM layers[24]. In hiAM-2.38 layers, however, the average activation frequency was significantly higher (7.5 ± 1.0 Hz, Fig. 6c). Also in hiAM-2.52 and hiAM-2.90 layers, reentrant activity with high activation frequencies could be induced (7.2 ± 0.8 and 7.9 ± 0.6 Hz, respectively, Supplementary Fig. 17). Interestingly, these activation frequencies very closely resemble those previously measured in the clinic in AF patients[25–27]. As expected from the faster CV in hiAM layers, reentrant circuit wavelength was greater in hiAM-2.38 layers than in hESC-AM layers (Fig. 6d). As a result, the arrhythmia complexity (expressed as number of reentrant circuits per cm²) was higher in hESC-AM layers compared with hiAM-2.38 layers

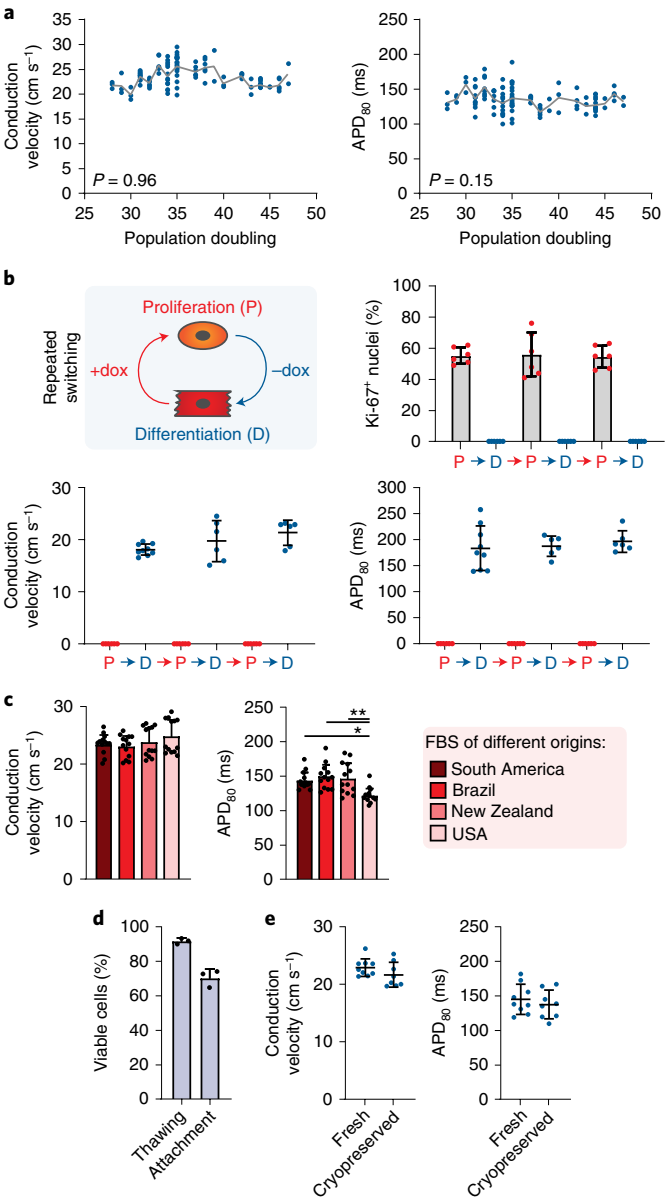

Fig. 5 | Robustness and effect of cryopreservation on hiAM differentiation capacity. a, CV and APD_{80} of hiAM-2.38 layers measured using optical voltage mapping over a broad range of PDs ($n = 111$). Stability of mean CV and APD_{80} at various PDs was tested using the Pearson correlation coefficient. **b**, Percentage of hiAM-2.38 with Ki-67$^+$ nuclei determined by immunocytochemistry, and CV and APD_{80} of hiAM-2.38 measured by optical voltage mapping during repeated switching between proliferation (P) and differentiation (D). $n = 6$–9 layers per time point from 3 independent experiments. **c**, Electrophysiological characteristics of hiAM-2.38 layers following differentiation using FBS of various origins and suppliers: South America (standard serum, S1860, Biowest), Brazil (10270098, Thermo Fisher), New Zealand (A3160901, Thermo Fisher) and USA (Premium FBS, 16000036, Thermo Fisher; $n = 13$ layers per group from 3 independent differentiations). $^*P < 0.05$, $^{**}P < 0.01$, one-way ANOVA with Tukey post-hoc analysis. **d**, Viability (determined by the Trypan Blue dye exclusion test) and attachment efficiency after thawing of hiAMs that had been cryopreserved at day 8 of differentiation ($n = 3$ batches each comprising 3 vials with 10^6 hiAMs per vial). **e**, Electrophysiological characteristics using optical voltage mapping of freshly differentiated hiAM-2.38 ($n = 9$ layers from 3 independent differentiations) vs cryopreserved differentiated hiAM-2.38 layers ($n = 8$ layers from 3 independent differentiations). In **b**–**e**, mean ± s.d.

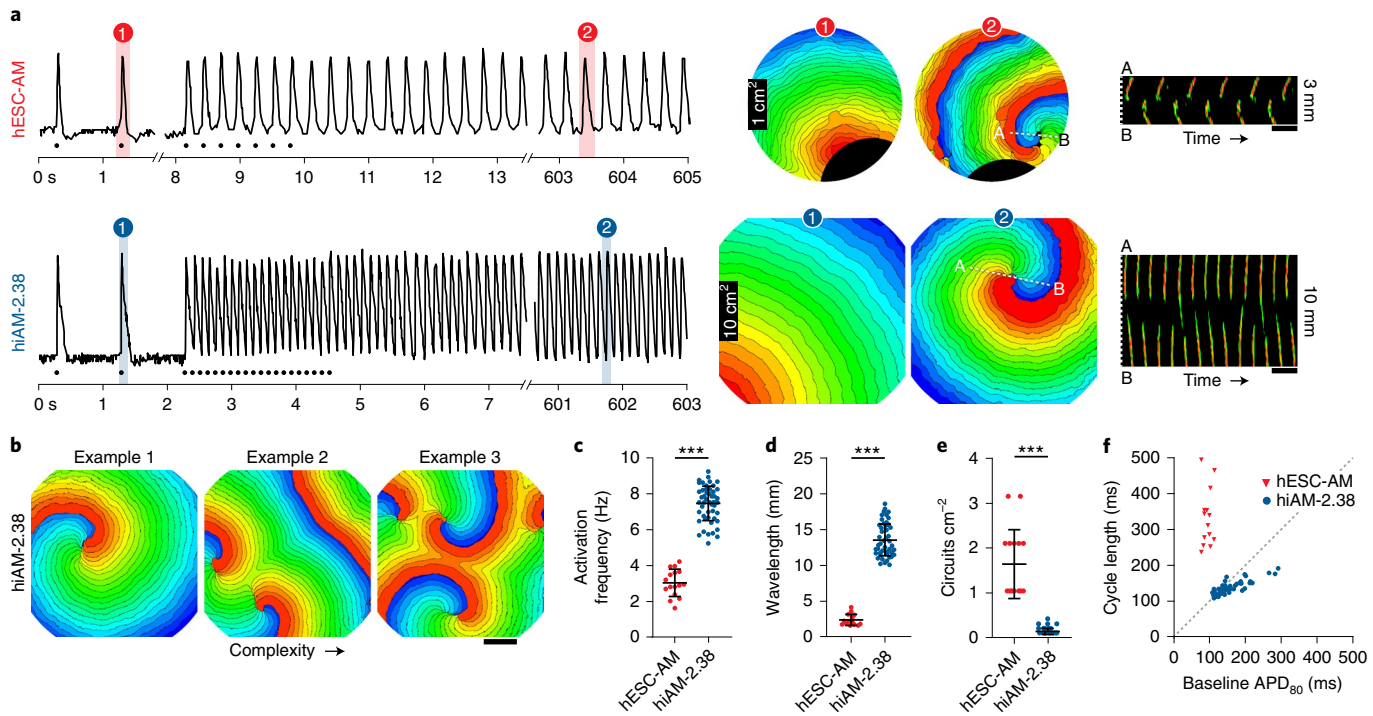

Fig. 6 | hESC-AM-based and hiAM-based atrial arrhythmia models. a, Optical voltage traces of reentrant circuit induction by high-frequency electrical pacing in 1 cm² hESC-AM and 10 cm² differentiated hiAM cultures (left). Corresponding activation maps before and after arrhythmia induction (middle). Line scan analysis between points A and B assessing reentrant circuit stability (right). Dots above the axes represent time points of electrical stimulation. Isochrones, 12 ms (hESC-AMs), 6 ms (hiAMs). Scale bar, 250 ms. **b**, Example of three 10 cm² hiAM-2.38 cultures following induction of reentrant activity of increasing complexity, that is, with an increasing number of reentrant circuits. Isochrones, 6 ms. Scale bar, 5 mm. **c**, Mean activation frequency of hESC-AM and hiAM cultures following induction of reentrant circuits. **d**, Mean wavelength of reentrant circuits. **e**, Arrhythmia complexity following stabilization expressed as number of reentrant circuits per cm². **f** Correlation between baseline APD_{80} and cycle length of induced reentrant circuits in hESC-AM and hiAM cultures. In **c**–**e**, mean ± s.d.; ***$P < 0.001$, unpaired *t*-test. In **c**–**f**, hESC-AM: $n = 16$ arrhythmia episodes from 7 independent cultures; hiAM-2.38: $n = 56$ independent cultures.

(Fig. 6e and Supplementary Video 4). Similar data were obtained in arrhythmic hiAM-2.52 and hiAM-2.90 layers (Supplementary Fig. 17). Moreover, in hESC-AM layers, the cycle length of reentrant circuits was much longer than the baseline APD_{80}, whereas in hiAMs these two parameters were very similar (Fig. 6f). Thus, reentrant circuits in hESC-AMs displayed a large temporal excitable gap compared with nearly no gap in hiAMs (Supplementary Fig. 17), which suggests that the slow CV in hESC-AM layers might be responsible for the low activation frequencies. Overall, hiAM monolayers better recapitulate the dynamics of human AF than hESC-AM monolayers do.

Effects of traditional antiarrhythmic drugs in hiAM-based AF model. The applicability of the hiAM-based AF model to study pharmacological interventions was tested using sotalol and flecainide, two antiarrhythmic drugs commonly used for rhythm control in AF patients[28–30]. Dimethylsulfoxide (DMSO), which served as solvent/vehicle for flecainide, did not affect the CV or APD in hiAM-2.38 layers subjected to 1 Hz electrical point stimulation. Increasing concentrations of sotalol also had no effect on CV, but dose-dependently increased the APD_{80} (Fig. 7a and Supplementary Fig. 18), as would be expected by its strong inhibitory effect on the rapid delayed rectifier K^+ current (I_{Kr})[31]. Flecainide, which mainly inhibits I_{Na} and I_{Kr}[32], decreased the CV and prolonged the APD_{80} in a dose-dependent matter. For each compound, 3 incremental doses were selected (DMSO: 0.01, 0.03 and 0.1%; sotalol: 3, 10 and 30 µM; flecainide 1, 3 and 10 µM), including clinically relevant concentrations (Fig. 7b).

Following the induction of stable reentry in hiAM-2.38 cultures, slow infusion of DMSO rarely resulted in termination of reentrant activity (Fig. 7c,d). DMSO also did not significantly alter the activation frequency, with the exception of the 0.01% dose, which slightly reduced the frequency (Fig. 7e). Sotalol infusion resulted in sporadic termination of reentrant activity, although termination rates for all doses did not significantly differ from those caused by DMSO treatment. The activation frequency, however, was significantly reduced for all sotalol concentrations in a dose-dependent manner. Finally, infusion of flecainide resulted in frequent arrhythmia termination at the two highest doses and also significantly reduced the activation frequency in a dose-dependent manner. These observations were also confirmed in hiAM-2.52 and hiAM-2.90 cultures (Supplementary Fig. 19). For these clones, 0.1% DMSO did not terminate any reentrant activity, whereas 10 µM flecainide resulted in frequent reentry termination. Thus, using the hiAM-based AF model, we were able to recapitulate the effects exerted by common antiarrhythmic drugs in AF patients at clinically relevant activation frequencies (Supplementary Video 5).

Discussion

Preclinical biomedical research across academia and industry has created a large demand for difficult-to-obtain human parenchymal cells to increase pathophysiological knowledge and to develop novel therapeutics. Although recent progress in human pluripotent stem cell (hPSC) technology has greatly advanced the development of human disease models, several challenges remain regarding

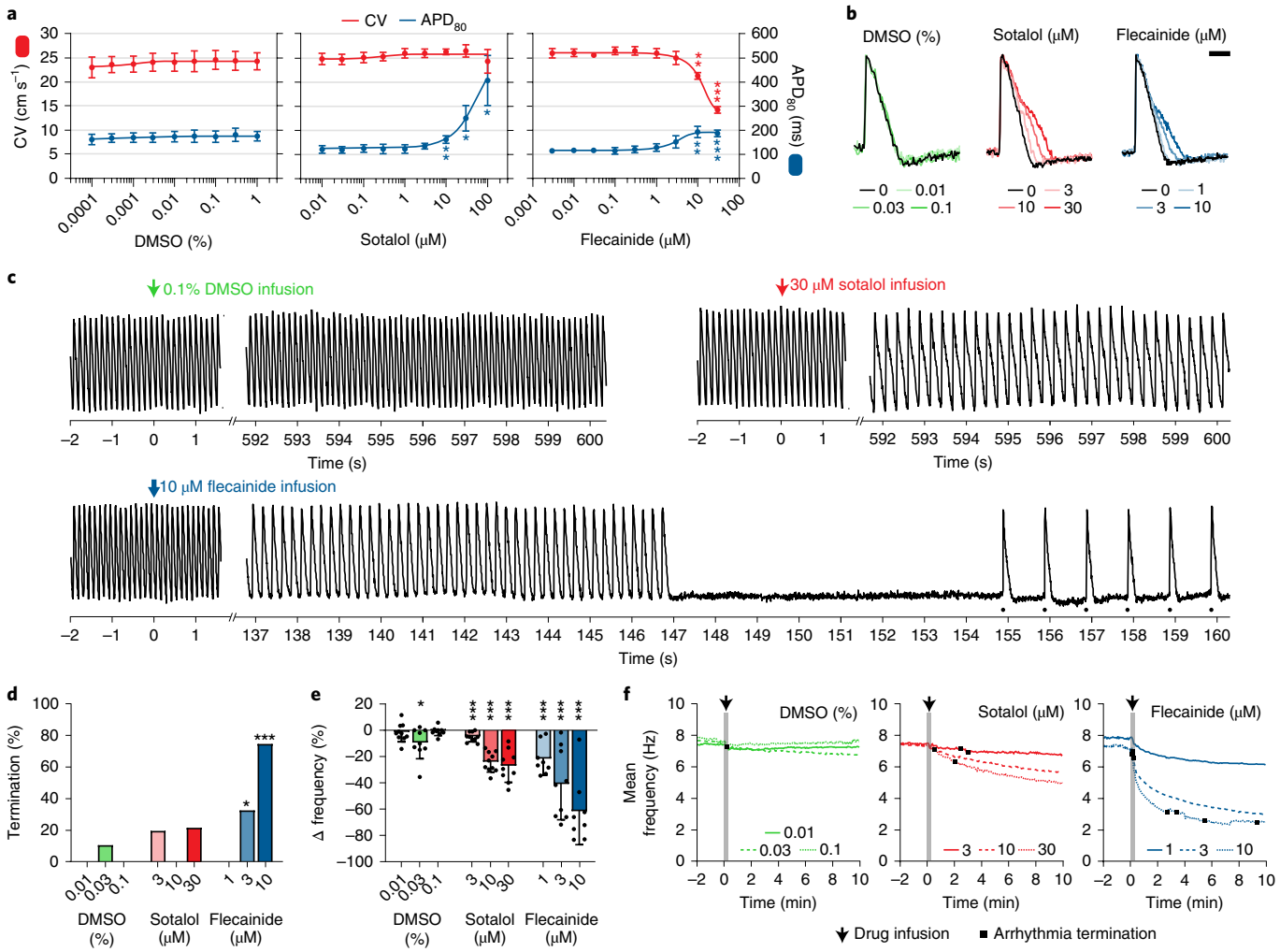

Fig. 7 | Effects of antiarrhythmic drugs in the hiAM-based atrial arrhythmia model. a, Effects of various concentrations of DMSO (solvent/vehicle control), sotalol or flecainide on CV (red, left axis) and APD_{80} (blue, right axis) in differentiated 2 cm^2 hiAM-2.38 cultures ($n = 5$ cultures for each compound). Repeated measures ANOVA with Tukey post-hoc analysis. **b**, Representative optical voltage traces of differentiated hiAM-2.38 in the presence of various concentrations of DMSO, sotalol or flecainide. Scale bar, 100 ms. **c**, Representative optical voltage traces of arrhythmic hiAM-2.38 cultures before and after infusion of DMSO (0.1%), sotalol (30 μM) or flecainide (10 μM). Dots above the lower axis represent time points of electrical stimulation. **d**, Rate of reentrant circuit termination in arrhythmic hiAM-2.38 cultures at 10 min after infusion of DMSO, sotalol or flecainide. The termination rates at the different sotalol and flecainide concentrations were compared with the termination rate of the combined DMSO concentrations using Chi-square test. **e**, Change (Δ) in activation frequency in arrhythmic hiAM-2.38 cultures following DMSO, sotalol or flecainide infusion (baseline compared to 10 min after infusion or before termination). Paired *t*-test. **f**, Continuous monitoring of mean activation frequency in arrhythmic hiAM-2.38 cultures before and after infusion of compounds at the indicated concentrations. For **c**–**f**, additional details on arrhythmia dynamics and termination mechanisms following drug infusion are provided in Supplementary Fig. 20. In **d**–**f**, $n = 8$–10 experiments for each dose, from 57 independent cultures. In **a** and **e**, mean ± s.d. In **a, d** and **e**: $^{*}P < 0.05$, $^{**}P < 0.01$, $^{***}P < 0.001$.

their scalability, representativeness and reproducibility. To address these issues, we developed an LV-based method for the conditional immortalization of primary mammalian cells. Here we have described the generation of standardized lines of human AMs with preserved cardiomyogenic differentiation capacity as a demonstration of the efficacy of this method. These so-called hiAM lines display strict control over proliferation and differentiation, allowing massive (that is, quadrillion-fold) cell expansion, followed by differentiation towards fully functional (that is, excitable and contractile) human AMs. The generation of these differentiation-competent human cardiomyocyte lines enabled the creation of human AF models that featured fibrillatory activity at clinically relevant frequencies, which could be terminated using antiarrhythmic drugs used in clinical practice.

The development of human cardiac muscle cell lines with preserved cardiomyogenic differentiation capacity has been the scope of several studies over the past decades[33,34]. Thus far, human cardiomyocyte lines failed to recapitulate the structural and functional characteristics of the primary cells from which they were derived. Here we show that this shortcoming can be overcome by imposing stringent control over SV40 LT expression in the target cells. The resulting hiAM lines allow straightforward production of contractile and excitable AMs in quantities not conceivable heretofore (for example, one hiAM line can generate the number of cardiomyocytes present in 100,000 human adult hearts). Due to the monoclonal nature of hiAM lines and the high efficiency with which the cells undergo cardiomyogenic differentiation, pure populations of human AMs can be produced with great ease. This provides a clear

advantage over derivation of AMs from hPSCs, which is a rather laborious and time-consuming multiphase process that generally includes a purification step[35,36] to select against the non-AMs remaining with current differentiation protocols[24,37,38]. Moreover, differentiation completely abolishes proliferation of hiAMs, while hPSC-derived cardiomyocytes still display some residual mitotic activity[39,40]. Additionally, our comparative transcriptome analyses show that differentiated hiAMs more closely match the gene expression profile of haAMs than hESC-AMs. Also, hPSC-AMs from different studies have a non-physiological average RMP of approximately −56 mV, reflecting their immature electrophysiological phenotype[24,37,38,41]. Differentiated hiAMs, in contrast, display an average RMP of −79 mV, which is well within the −70 to −85 mV range reported for haAMs[42–44]. The depolarized membranes of hPSC-AMs probably contribute to the slow AP propagation observed in confluent 2/3D cultures of these cells[24,45,46]. Above −70 mV, a considerable fraction of Na^+ channels becomes inactivated, resulting in a decrease in AP upstroke velocity and a consequential reduction in CV. Although the CV in hiAM layers is significantly faster than in layers of hPSC-AMs (up to 30 cm s^{-1} vs up to 2.5 cm s^{-1}), it is still slower than the 60–75 cm s^{-1} reached in human adult atrial tissue[47]. This can, at least in part, be explained by the absence of anisotropic organization and neurohumoural regulation in the monolayers of differentiated hiAMs[48], providing a rationale for the future application of in vitro patterning technology to create cables/sheets of uniaxially aligned hiAMs and thereby increase the (longitudinal) CV in these structures along with neurohormonal stimulation.

The basic electrophysiological properties of hiAMs and hPSC-AMs also directly influence their applicability for AF modelling. The first report[24] of reentrant circuit induction in (non-purified) hESC-AM layers showed activation at a mean frequency of 3.2 Hz, which is very similar to the 3.0 Hz we found in our (purified) hESC-AM layers, but much lower than the 7.5 Hz in hiAM layers. For reference, activation frequencies measured in AF patients range between 6 to 8 Hz, depending on the type of AF[25–27]. When studying the influence of antiarrhythmic drugs on reentry dynamics, activation frequencies resembling clinical AF are critical because of (reverse) rate-dependent effects. For instance, the I_{Na}-blocking activity of flecainide is increased at higher activation frequencies[49], which could explain why termination of reentry using 10 μM flecainide was possible in the majority of hiAM layers, while this was previously not successful in hESC-AM layers[24]. As our hiAM-based AF model displays the main electrophysiological phenomena driving AF and provides new possibilities over existing models for studies into arrhythmia dynamics and antiarrhythmic drug discovery, a future extension would be to move towards more advanced 3D in vitro models of AF. Atrium-like 3D tissues have recently been generated using hPSC-AMs[46,50,51], but due to their small size (largest dimension ≤5 mm), they cannot accommodate reentrant circuits with characteristics similar to human AF. Advances in bioprinting technology have already demonstrated the feasibility of creating large and complex (cardiac) scaffolds required for tissue engineering of whole human hearts[52]. The main limiting factor for the creation of such large tissue constructs to date has been the difficulty associated with generating the hundreds of millions/billions of well-differentiated cells necessary to populate these constructs. Although a recent report has shown that this problem may at least be partially overcome by a new method allowing the expansion of hiPSC-derived ventricular myocytes[40], it remains to be seen whether it can also induce multiplication of hPSC-AMs. Accordingly, the extensive scalability, cost-effectiveness and robustness of hiAM differentiation might provide a new impulse to create larger human atrial constructs for disease modelling, mechanistic studies and drug screening.

The ability to generate large numbers of differentiated hiAMs in an effective and robust manner may furthermore open the possibility to use them for biopharmaceutical production of, for instance, cardiomyocyte-derived exosomes and cardiokines[53]. The latter property, together with the monoclonal origin of hiAMs and the high controllability of their phenotype and gene expression profile, makes these cells particularly suitable for (very) high-resolution 'omics' studies by obviating the need for cell selection and providing plentiful input material. This offers new possibilities: (1) to identify yet unknown factors involved in cardiomyocyte proliferation and differentiation, and (2) to find novel therapeutic targets, especially when combined with (opto)genetic, pharmaceutical, chemical or physical interventions to mimic disease states.

Although hiAM lines have many advantages over current AM sources, their suitability for regenerative purposes is limited due to the use of an integrating LV encoding an oncoprotein (that is, SV40 LT) for (conditional) immortalization, which harbours the risk of tumour formation. hiAMs may, however, still be applied in animal models to optimize cardiac cell therapy, and may help to find new leads for endogenous induction of myocardial regeneration through stimulation of cardiomyocyte proliferation in situ. Although the high controllability and synchronicity of the transition from proliferation to differentiation could make hiAMs an excellent model for studying the molecular mechanisms underlying these transitions, they will not fully represent the natural course of events due to the very nature (that is, viral oncoprotein-dependent conditional immortalized state) of the cells. Moreover, the aneuploid status of hiAMs, which is associated with expression of SV40 LT[54], might limit certain applications with high sensitivity to potential gene imbalances. Nevertheless, this status did not result in apparent deviations from the AM phenotype on the basis of our comprehensive comparative analyses. In addition, the initial investment associated with the development of these cell lines, as well as the need for access to primary cardiac material, make the conditional immortalization technique less suited than hiPSC technology for widescale patient-specific disease modelling. Still, using gene delivery or genome editing technologies, hiAM sublines with genetic modifications could easily be created, allowing studying of the effects of these alterations in a highly standardized cell system. For instance, as described in the Supplementary Results, we could show that differentiated hiAMs with lentiviral short hairpin RNA-mediated knockdown of TBX5 expression display very similar disturbances of Ca^{2+} dynamics as observed in Holt-Oram syndrome (see Supplementary Fig. 21). The ease with which hiAMs can be genetically modified makes it possible to perform comprehensive mechanistic studies mimicking the different types of atrial disease[55], allowing dissection of the precise molecular signatures of the diverse atrial cardiomyopathies, thereby fostering the development of novel preventive anti-AF therapies.

In summary, the conditional immortalization of hfAMs has enabled the creation of fully differentiation-competent lines of human cardiomyocytes as well as of human in vitro models of AF displaying clinically relevant features, which can be readily genetically modified to also mimic specific inherited atrial cardiomyopathies. This provides proof-of-concept of a versatile new method to produce, in a simple and rapid manner, massive numbers of authentic human cells for the development of representative human in vitro models for animal-free disease investigation, target identification, along with drug discovery and therapeutic testing.

Methods

LV production. To generate vesicular stomatitis virus G protein-pseudotyped LV.iMHCK7.LT-WT particles, near confluent monolayers of 293T cells[56] were transfected with LV shuttle construct pLV.iMHCK7.LT-WT (Supplementary Fig. 1) and the packaging plasmids psPAX2 (Addgene, plasmid number: 12260) and pLP/VSVG (Thermo Fisher, K497500) at a molar ratio of 2:1:1. pLV.iMHCK7.LT-WT is identical to pLV.iMHCK7.LT-*ts*A58[7], except for the replacement of the coding sequence of the temperature-sensitive SV40 LT mutant *ts*A58 with that of wild-type LT. The 293T cells were cultured in high-glucose Dulbecco's modified

Eagle's medium (DMEM, Thermo Fisher, 41966) with 10% FBS (Thermo Fisher, 10270-106). The transfection mixture, consisting of 35 µg plasmid DNA and 105 µg linear 25 kDa polyethyleneimine (Polysciences, 23966) in 2 ml 150 mM NaCl per 175 cm^2 cell culture flask (Greiner Bio-One, 660160), was directly added to the culture medium. Approximately 16 h later, the transfection medium was replaced with 15 ml fresh high-glucose DMEM supplemented with 5% FBS and 25 mM HEPES-NaOH (pH 7.4). At ~48 h after the start of the transfection procedure, the culture supernatants were collected, cleared from cellular debris by centrifugation at r.t. for 10 min at 3,750 × *g* and subsequent filtration through 0.45-µm-pore-size, 33-mm-diameter polyethersulfone Millex-HP syringe filters (Merck Millipore, SLHP033RB). The LV particles were further purified and concentrated by underlaying 30 ml vector suspension in a 38.5 ml polypropylene ultracentrifuge tube (Beckman Coulter, 326823) with 5 ml 20% (wt/vol) sucrose in phosphate-buffered saline (PBS) and subsequent centrifugation with slow acceleration and without braking at 15,000 revolutions per minute in an SW32 rotor (Beckman Coulter, 369650) for 2 h at 4 °C. Next, the supernatants were discarded and each pellet was suspended in 500 µl PBS-1% bovine serum albumin (Sigma-Aldrich, A2153) by overnight incubation with gentle shaking at 4 °C. The concentrated vector suspension was divided on ice in 100 µl aliquots for storage at −80 °C. LV.iMHCK7.SV40-LT-WT particles can be obtained by academic research groups under a material transfer agreement (for enquiries, contact hiAM@lumc.nl).

Ethics statement. Human foetal cardiac samples were obtained after elective abortions and with written informed consent. Donors were not incentivized/compensated. The samples were delivered to the researcher without any information except for the age of the foetus to guarantee full anonymity of the donors. This study was conducted with approval of the institutional review board of the Leiden University Medical Center (P08.087) and in compliance with the International Code of Medical Ethics of the World Medical Association.

Isolation and culture of hfAMs. The atria were separated from the ventricles of the foetal heart, minced into pieces of ~1 mm^2 and dissociated by 2 successive 30 min treatments with collagenase type I (225 U ml^{-1}, Worthington Biochemical, LS004196) and DNase I (20 U ml^{-1}, Sigma-Aldrich, DN25) under gentle agitation at 37 °C. Cells were pelleted by centrifugation for 10 min at 160 × *g* and r.t. The supernatant was removed and cells were resuspended in Ham's F10 medium (Thermo Fisher, 11550) supplemented with 100 U ml^{-1} penicillin and 100 µg ml^{-1} streptomycin (Thermo Fisher, 15070-063), 10% heat-inactivated FBS (Thermo Fisher, 10500) and 10% heat-inactivated horse serum (Thermo Fisher, 26050). The cell suspension was transferred to uncoated Primaria culture dishes (Corning, 353803) and incubated for 75 min at 37 °C in a humidified atmosphere of 95% air:5% CO_2 to allow preferential attachment of non-cardiomyocytes. Unattached cells were filtered through a nylon cell strainer (Corning, 431751) containing evenly spaced 70 µm mesh pores and seeded for experiments. For conditional immortalization, 10^4 cells per cm^2 were seeded in a 6-well culture plate (Corning, 3506) coated with fibronectin from bovine plasma (100 µg ml^{-1}, Sigma-Aldrich, F1141). For immunocytochemistry and patch clamping, 5×10^4 and 2.5×10^4 cells per cm^2 were respectively seeded on fibronectin-coated glass coverslips in 24-well plates (Corning, 3524).

Conditional immortalization and selection of hiAM monoclones. The human foetal atrial cell mixture was transduced with 2.5 µl concentrated LV.iMHCK7.SV40-LT-WT stock (that is, the vector yield of 1.65×10^5 producer cells), following 2 days recovery. Three days following transduction, the culture medium was changed to hiAM proliferation medium, consisting of advanced DMEM/F-12 (Thermo Fisher, 12634), 2 mM GlutaMAX (Thermo Fisher, 35050061), 2% FBS (Biowest, S1810), 100 U ml^{-1} penicillin and 100 µg ml^{-1} streptomycin supplemented with 100 ng ml^{-1} doxycycline hyclate (Sigma-Aldrich, D9891) to induce SV40 LT expression. After the observation of cell proliferation, cells were detached using Accutase (BD Biosciences, 561527) and plated at a density of 10 cells per cm^2 in 145-mm-diameter culture dishes (Greiner Bio-One, P7737) in the presence of hiAM proliferation medium. These dishes were maintained for 2–3 weeks at 37 °C in a humidified atmosphere of 95% air:5% CO_2 until colonies of 100–200 cells were observed. Individual colonies were then isolated with the aid of glass cloning cylinders (6 mm diameter, Corning, 3166-6) and treated with Accutase, after which the collection of cells inside each cylinder was transferred to single wells of a 48-well plate (Corning, 3548) in hiAM proliferation medium. Isolated colonies were given a unique number, expanded up to 10^6 cells and graded on the basis of their proliferative and differentiation qualities. The conditional immortalization was considered successful for hiAM monoclones that: (1) when given dox-containing hiAM proliferation medium proliferated beyond 15 PDs with a PD time shorter than 120 h and (2) in the presence of dox-free hiAM differentiation medium (see below): (a) stopped proliferating and gradually acquired a cardiomyocyte-like phase-contrast appearance, (b) lost proliferation marker Ki-67 expression and eventually consisted of >50% TNNT2-positive cells as assessed by immunocytochemistry and (c) were electrically excitable with a minimal CV of 10 cm s^{-1} and maximal APD_{80} of 300 ms following optical voltage mapping of 1 cm^2 monolayers ≥12 days after dox removal. All selection criteria, including corresponding drop-off rates per criterion, can be found in Supplementary Fig. 1.

Proliferation and differentiation of hiAMs. Proliferating hiAMs were cultured in uncoated TC-treated CELLSTAR flasks (Greiner Bio-One, 6901755, 658175, 660175) in the aforementioned hiAM proliferation medium. Culture medium was refreshed every 2–3 d. When confluency approached 90%, proliferating hiAMs were subjected to a 10 min treatment with Accutase at 37 °C and carefully triturated into a (nearly) single-cell suspension. Next, the cells were pelleted by centrifugation at 160 × *g* for 5 min at r.t. and transferred in a 1:2 to 1:4 ratio to new culture flasks for further multiplication, or seeded in appropriate culture plates for cardiomyogenic differentiation. Differentiation of hiAMs was performed in fibronectin-coated culture plates and initiated by changing the hiAM proliferation medium to hiAM differentiation medium, consisting of advanced DMEM/F-12 (Thermo Fisher, 12634), 2 mM GlutaMAX and 2% Biowest FBS. Starting at day 4 of differentiation (the initiation of differentiation being day 0), hiAM differentiation medium was supplemented with 20 ng ml^{-1} triiodo-L-thyronine (T3) hormone (Sigma-Aldrich, T6397), 400 ng ml^{-1} dexamethasone (Centrafarm, 55091), 8 µM LF3 (Selleck Chemicals, S8474) or 10 µM ICRT14 (Sigma-Aldrich, SML0203) and 10 µM phenylephrine (Sigma-Aldrich, P6126). Culture medium was refreshed every 2 days during differentiation. At day 12 of differentiation, the hiAMs were considered fully differentiated as at that time point, CV and APD reached their plateau values. All experiments in this study were performed between days 12 and 15 after initiation of differentiation.

Proliferation assay. To assess the proliferation rates of individual hiAM clones in the presence of dox, 2×10^3 cells per cm^2 were seeded in multiple 100-mm-diameter culture dishes (Corning, 430167). At 48 h intervals following culture initiation, cells were detached using Accutase, collected in hiAM proliferation medium and mixed in a 1:1 ratio with 0.4% Trypan Blue (Sigma-Aldrich, T8154). Following brief incubation, cells were counted using a CytoSMART cell counter (Corning). PD times were calculated by fitting data with an exponential growth equation using GraphPad Prism v8.0.1.

Immunocytochemistry and image quantification. hfAMs and hiAMs were seeded at a density of 8×10^4 cells per cm^2 on fibronectin-coated coverslips before fixation with 4% buffered formaldehyde (Added Pharma, 14144751) for 30 min at 4 °C. Cells were permeabilized by incubation with PBS/0.1% Triton X-100 (Sigma-Aldrich, X100) for 10 min, incubated with PBS/10% normal donkey serum (NDS, Sigma-Aldrich, D9663) for 30 min to block non-specific background staining and subsequently exposed to the primary antibody in PBS containing 0.5% NDS for 2 h, all at r.t. After each treatment, cells were washed 3 times with PBS. Secondary antibody incubation was performed in PBS containing 0.5% NDS for 45 min and nuclei were stained for 10 min with Hoechst 33342 solution (Thermo Fisher, H-3570) diluted 1:1,000 in PBS. For an overview of the antibodies and the dilutions at which they were applied, see Supplementary Table 5. Coverslips were mounted on StarFrost slides (VWR, KNITVS112731FEA.01) using VECTASHIELD (Vector Laboratories, H-1000-10) and imaged with an Eclipse 80i upright microscope (during clone screening, Nikon Instruments) or TCS SP8 White Light laser confocal microscope (during characterization, Leica Microsystems). Details on the use of the fluorescence microscopes are provided in the Supplementary Methods.

Counting of Ki-67$^+$ nuclei on the basis of mean grey values was performed using ImageJ (v1.52a, http://imagej.nih.gov/). For hiAMs, all Hoechst 33342-positive nuclei were analysed. In the case of the primary hfAMs, only the Nkx-2.5-positive nuclei were considered to avoid analysis of the non-cardiomyocytes present in the samples. The mean grey value of each nucleus was compared to a threshold to distinguish between positive and negative nuclei. Sarcomere length was calculated by measuring the *z*-line distance of multiple adjacent sarcomeres in cell layers stained for ACTN2 (LAS X, v3.6.0, Leica Microsystems).

Western blotting. Adherent hiAMs were lysed on ice in RIPA buffer (50 mM Tris-HCl (pH 8.0), 150 mM NaCl, 1% NP-40, 0.5% sodium deoxycholate, 0.1% sodium dodecyl sulfate) supplemented with Roche cOmplete Mini Protease Inhibitor Cocktail (Sigma-Aldrich, 4693124001). The lysate was passed 3 times through a 30-gauge needle (BD Biosciences, 324826), centrifuged at 16,000 × *g* for 20 min at 4 °C, after which the supernatant was collected and stored at −80 °C. Protein concentrations in the cleared lysates were determined using the Pierce BCA protein assay kit (Thermo Fisher, 23225). Proteins were size-fractionated in Invitrogen Bolt 10% Bis-Tris Plus gels (Thermo Fisher, NW00102BOX) and transferred to Amersham Hybond P 0.45 µm polyvinylidene difluoride membranes (GE Healthcare, GEHE10600023) by wet electroblotting using a Bolt Mini Blot module (Thermo Fisher). Membranes were incubated for 1 h in 2% ECL Prime blocking reagent (GE Healthcare, RPN418) dissolved in Tris-based saline/0.1% Tween 20 (TBST). Membranes were then incubated for 1 h with the primary antibody in TBST/2% ECL Prime blocking reagent, washed 5 times with TBST and incubated for 1 h with corresponding horseradish peroxidase-conjugated secondary antibodies. Information on the antibodies used can be found in Supplementary Table 5. Following 5 washes with TBST, membranes were covered with SuperSignal West Femto Maximum Sensitivity Substrate (Thermo Fisher, 34095) and chemiluminescence was measured using the ChemiDoc Touch imaging system (Bio-Rad Laboratories) or iBright FL1500 imaging system

(Thermo Fisher). In some cases, the blot was stripped following imaging using Restore PLUS western blot stripping buffer (Thermo Fisher, 46430) for an additional round of immunostaining. Protein levels were quantified with the aid of Image Lab (v6.0.1, Bio-Rad Laboratories) or the on-instrument software of the iBright FL1500 imaging system, using levels of the housekeeping proteins and loading controls glyceraldehyde 3-phosphate dehydrogenase (GAPDH) or lamin A/C (LMNA) for normalization purposes.

RNA sequencing of hiAM proliferation vs differentiation. Total RNA was extracted from proliferating and differentiated hiAMs seeded at a density of 10^5 cells per cm^2 (10^6 cells per sample) using the RNeasy Plus mini kit (Qiagen, 74104) according to the manufacturer's instructions. RNA sequencing was performed by GenomeScan (Leiden, the Netherlands). Quality and integrity of the RNA were confirmed using a 2100 Bioanalyzer Instrument (Agilent Technologies), with a measured RNA quality number of 10.0 for all samples. Library preparation was performed using the NEBNext Ultra II Directional RNA Library Prep Kit for Illumina in combination with the NEBNext Poly(A) mRNA Magnetic Isolation Module (New England Biolabs, E7765). Sample quality and yield after complementary DNA synthesis and polymerase chain reaction enrichment were measured with the bioanalyzer (average size range, 445–524 base pairs (bp)). Clustering and DNA sequencing (50–82 million 150 bp paired-end reads) using the NovaSeq6000 DNA sequencer (Illumina) was performed according to the manufacturer's protocols. Image analysis, base calling and quality check were performed with the Illumina data analysis pipeline RTA3.4.4 and Bcl2fastq (v2.20). Before alignment, the reads were trimmed for adaptor sequences using Trimmomatic (v0.30). Reads were aligned to the *Homo sapiens* reference genome (GRCh37.75) using Tophat (v2.0.14) and read counts were determined using HTSeq (v0.6.1p1). Additionally, TPM values were calculated to compare gene expression levels between groups. Differential gene expression (Wald test) was assessed by analysing read counts with the DESeq2 package (v1.14.1) in the R platform (v3.3.0). Genes with an absolute $\log_2$ fold change >1.0 (that is, >2-fold absolute change) and FDR-corrected $P < 0.001$ were considered differentially expressed. Comparison of differentially expressed genes (DEGs) between clones was limited to genes with >1 TPM in the proliferative state or at day 12 of cardiomyogenic differentiation to exclude DEGs with very low overall expression. Gene set enrichment analysis was performed in DAVID (v6.8).

RNA sequencing of hESC-AMs and hiAMs. Total RNA was extracted from hESC-AMs (10^6 cells per sample) using the NucleoSpin RNA kit (Macherey-Nagel, 740955) according to the manufacturer's instructions. Total RNA extraction from hiAMs has been described above. Libraries were generated from 200 ng RNA using the KAPA-RNA HyperPrep kit with RiboErase (Roche, 8098131702) to remove ribosomal RNA, according to the manufacturer's instructions. Library amplification was performed with 11 cycles, after which the size distribution was determined with a 2100 Bioanalyzer instrument. Paired-end library sequencing was performed with the NextSeq500 sequencing system (Illumina). Trimming of the reads and alignment was performed with seq2science (v0.4.0, available in Zenodo, https://doi.org/10.5281/zenodo.4451349). In short, Fastp[57] (v0.20.1) trimmed the low quality 3' ends and Salmon[58] (v1.3.0) quant aligned the reads to the GRCh38.p13 genome from Ensembl, after which tximeta[59] (v1.4.3) generated the gene expression matrix. The counts per million (CPM) were $\log_1$p-transformed. The foetal dataset published by Cui et al.[19] was retrieved as count matrix and the mean expression was calculated per tissue type. The 2,000 most variable genes within this dataset were determined with the variance-stabilized transformation method in Seurat[60] (v3). The selection of the most variable genes in the GTEx portal dataset[20] was performed by taking the genes with a coefficient of variation >2. Differential gene expression analysis (Wald test) between hESC-AMs and hiAMs was performed with the R package DESeq2[61] (v1.22.2). The differential gene list was filtered for a $\log_2$ fold change >1 and *P*-adjusted value <0.01 (4,145 significant differential genes in total), and visualized with pheatmap (v1.0.12). To establish whether there were significant differences in specific gene list ranks between the samples, the Wilcoxon signed-rank test (two-sided) was used in pairwise comparisons.

Generation of hESC-AMs. NKX2.5$^{eGFP/+}$-COUP-TFII$^{mCherry/+}$ hESCs, as previously described[35], were maintained as undifferentiated colonies in Essential 8 medium (Thermo Fisher, A1517001) on vitronectin-coated (Thermo Fisher, A14700) culture plastics. Differentiation of these cells to AMs was performed using the previously described spin embryoid body protocol with retinoic acid treatment[35,41]. To generate pure populations of hESC-AMs, eGFP- and mCherry-double positive cells were purified at around day 17 of differentiation using a Sony Biotechnology SH800 flow cytometer after exclusion of dead cells and debris according to side and forward scatter. After sorting, cells were suspended in TID medium containing T3 hormone, insulin-like growth factor 1 and dexamethasone[62] and transferred to vitronectin-coated 48-well culture plates to establish confluent monolayers. Optical voltage mapping of hESC-AMs was performed 5–11 days after replating.

Cellular electrophysiology. Differentiated hiAMs were dissociated by incubation with a 5 U ml^{-1} papain (Worthington Biochemical, LS003127) and 1 mM L-cysteine (Sigma-Aldrich, C6852) solution in PBS for 10 min at 37 °C. Next, an equal volume of stop solution was added, consisting of 1 mg ml^{-1} soybean trypsin inhibitor (Sigma-Aldrich, T9253) and 40 µg ml^{-1} DNase I in PBS. Cells were pelleted by centrifugation at 160×*g* for 5 min at r.t., plated at densities of 3×10^4 to 6×10^4 cells per cm^2 on fibronectin-coated 12-mm-diameter glass coverslips (VWR, 631-1577) and measured over the 3 following days.

Single-cell APs and membrane currents were recorded using Axopatch 200B and MultiClamp 700B amplifiers (Molecular Devices). Signals were low-pass filtered at 5 kHz cut-off frequency and digitized at 40 and 20 kHz for APs and membrane currents, respectively. Data acquisition and analysis were accomplished with pClamp (v10.7, Molecular Devices) and custom-made software. Series resistance was compensated by ≥80%. Patch pipettes were pulled from borosilicate glass (Harvard apparatus) and had resistances of 2.0–3.0 MΩ after filling with the indicated solutions. Potentials were corrected for the calculated liquid junction potential[63]. Cell membrane capacitance (C_m) was estimated by dividing the time constant of the decay of the capacitive transient in response to 5 mV hyperpolarizing voltage clamp steps from −40 mV by the series resistance.

APs were recorded using the amphotericin-perforated patch-clamp technique at 36 ± 0.2 °C. The bath solution was a modified Tyrode's solution containing (in mM): 140 NaCl, 5.4 KCl, 1.8 $CaCl_2$, 1.0 $MgCl_2$, 5.5 glucose and 5.0 HEPES-NaOH (pH 7.4). The pipette solution contained (in mM): 125 K-gluconate, 20 KCl, 5.0 NaCl, 0.44 amphotericin B (Sigma-Aldrich, A2411) and 10 HEPES-KOH (pH 7.2). APs were elicited at 1 Hz by 3 ms, ~1.2× threshold current pulses through the patch pipette. Parameters from ten consecutive APs were averaged. APs from haAMs were measured in non-depolarized single rod-shaped cardiomyocytes[64], which were isolated for a previous study[65]. In short, cells were enzymatically isolated with the chunk method from left atrial appendages as described previously[65]. These appendages were obtained from patients in sinus rhythm undergoing cardiac surgery (coronary bypass grafting or valve surgery), and included in the multicentre PREDICT AF study[66]. The patient characteristics are as reported previously[65]. Details on the Na^+ and K^+ current recordings in hiAMs are provided in the Supplementary Methods.

Optical voltage mapping. To assess AP properties and propagation in monolayers, hiAMs were seeded in fibronectin-coated 48-well, 24-well or 6-well culture plates at a density of 4×10^5 cells per cm^2 and differentiated as described. Alternatively, hESC-AMs were seeded at a density of 5.8×10^5 cells per cm^2 in vitronectin-coated 48-well culture plates. Cell layers of hiAMs or hESC-AMs were incubated with 8 µM di-4-ANEPPS (Thermo Fisher, D1119) in DMEM/F-12 (Thermo Fisher, 11039) for 10 min in a humidified 95% air:5% CO_2 incubator at 37 °C. Following incubation, the medium was changed to fresh DMEM/F-12 and cells were placed on a 37 °C warming plate for the duration of the experiment.

During optical voltage mapping, excitation light (525 ± 25 nm) was delivered by a halogen arc-lamp through epi-illumination. Emission light passed through a dichroic mirror and a long-pass emission filter (>590 nm). Signals were acquired using a 100×100 pixels complementary metal oxide semiconductor camera (MiCAM05-Ultima, SciMedia) at a spatial resolution of 165 (for 48- and 24-well plates) or 250 (for 6-well plates) µm per pixel, and a temporal resolution between 2 and 6 ms per frame depending on the type and duration of the experiment. Acquisition times varied between 4 and 12 s for characterization studies, and up to 2 min for arrhythmia studies.

Data were analysed using BrainVision Analyzer (v16.04.20, BrainVision). Signals were averaged with those of the 8 nearest neighbouring pixels to minimize noise artefacts. CV, APD and activation frequency were determined at a minimum of 5 different vectors/locations equally distributed throughout the culture. Arrhythmia wavelength was calculated by multiplying average CV and APD_{90}. Temporal excitation gap was calculated by subtracting APD_{90} during arrhythmic activation from the cycle length. Activation frequency over time was determined by analysing peak to peak intervals through a custom MATLAB (vR2016a, MathWorks) script on high-pass filtered data at selected locations in the culture.

Electrical stimulation and arrhythmia induction. Electrical point stimulation during optical voltage mapping was performed using an epoxy-coated bipolar platinum electrode, delivering 8 V, 10 ms square pulses. The electrode was connected to an STG 2004 stimulus generator (Multi Channel Systems) driven by MC Stimulus II software (v3.5.0, Multi Channel Systems). Baseline AP properties and propagation were calculated during 1 Hz electrical pacing (that is, 1,000 ms cycle length). Restitution was calculated by pacing at a cycle length of 1,000 ms (S1), followed by an additional stimulus (S2) at a variable cycle length. Arrhythmia induction was performed by delivering 20 to 40 stimuli at the shortest cycle length at which 1:1 capture was maintained (range 90–180 ms), generally starting with a cycle length equal to the APD_{80}.

Arrhythmia studies and drug interventions. To determine relevant compound dosage, flecainide acetate salt (Sigma-Aldrich, F6777) dissolved in DMSO (CryoMACS, Miltenyi Biotec, 170-076-303), sotalol hydrochloride (Sigma-Aldrich, S0278) dissolved in demineralized water and DMSO (solvent/vehicle control), were tested on 2 cm^2 hiAM layers at increasing doses during optical voltage mapping, until loss of excitability. For each compound, 3 escalating doses were chosen, to include various effect sizes in a clinically relevant range.

Induced reentrant circuits were monitored for 5 min to confirm stability before compounds were infused to study their effect on reentrant circuit characteristics. Flecainide, sotalol or DMSO as control, all at 3 concentrations, were slowly infused in a 1:1 volume ratio into cultures with reentrant circuits during optical voltage mapping using an infusion pump (Acromed Medical Systems) that controlled infusion rate and volume (3 ml at 0.16 ml s^{-1}). Cultures were continuously monitored from 2 min before drug infusion until 10 min after the start of the drug treatment.

Cryopreservation. hiAMs at day 8 of cardiomyogenic differentiation were dissociated by papain treatment, pelleted by centrifugation and resuspended in cold (4 °C) culture medium. Next, an equal volume of ice-cold 80% FBS/20% DMSO was added dropwise to the suspension, after which cryovials containing 10^6 cells per ml were frozen to −80 °C at a rate of −1 °C min^{-1}. Twenty-four hours later, the cells were placed in nitrogen vapour for long-term storage. Cells were thawed by swirling vials in a 37 °C bath, immediately followed by dropwise addition of cold (4 °C) culture medium until a 10-fold dilution was reached. Cells were pelleted by centrifugation, resuspended in supplemented hiAM differentiation medium and cultured for 6 days in this medium to complete differentiation. Cell viability after dissociation and after thawing, as well as replating efficiency of the cells were determined by 0.4% Trypan Blue staining (1:1 ratio) and manual counting using a haemocytometer.

Statistics and reproducibility. Statistical analyses were performed using GraphPad Prism v8.0.1. Data are presented as mean ± s.d. or mean ± s.e.m., unless otherwise indicated. Normally distributed data between independent groups was tested for statistical significance using unpaired *t*-test (2 groups) or one-way analysis of variance (ANOVA) with Tukey or Dunnett post-hoc analysis (3 or more groups). Dependent groups were tested using paired *t*-test (2 groups) or repeated measures one-way ANOVA with Tukey or Dunnett post-hoc analysis (3 or more groups). Non-normally distributed independent data were compared using the Mann–Whitney test. Non-normally distributed dependent data of multiple groups were compared using the Friedman test with Dunn post-hoc analysis. The stability of mean CV and APD at various PDs was tested by calculating the Pearson correlation coefficient. Rates of reentrant activity termination were compared between groups using Chi-square test. All testing performed was two-sided. Statistical significance was expressed as follows: $^*P<0.05$, $^{**}P<0.01$, $^{***}P<0.001$. Precise *P* values can be found in Supplementary Data File 3. Representative micrographs were chosen from a number of images (generally $n\geq3$), on the basis of multiple independent differentiations.

Reporting Summary. Further information on research design is available in the Nature Research Reporting Summary linked to this article.

Data availability

The main data supporting the results in this study are available within the paper and its Supplementary Information. Certain raw and analysed datasets generated during the study are too large to be publicly shared, but they are available for research purposes from the corresponding author on reasonable request. The RNA-sequencing data are available at the NCBI's Gene Expression Omnibus (GEO) under GEO accession numbers GSE156824 and GSE178473. The whole-genome-sequencing data are available under BioProject accession number PRJNA760786.

Received: 20 October 2020; Accepted: 29 October 2021;
Published online: 06 January 2022

References

1. Robinson, N. B. et al. The current state of animal models in research: a review. *Int. J. Surg.* **72**, 9–13 (2019).
2. Ruijtenberg, S. & van den Heuvel, S. Coordinating cell proliferation and differentiation: antagonism between cell cycle regulators and cell type-specific gene expression. *Cell Cycle* **15**, 196–212 (2016).
3. Thomson, J. A. et al. Embryonic stem cell lines derived from human blastocysts. *Science* **282**, 1145–1147 (1998).
4. Takahashi, K. et al. Induction of pluripotent stem cells from adult human fibroblasts by defined factors. *Cell* **131**, 861–872 (2007).
5. Yu, J. et al. Induced pluripotent stem cell lines derived from human somatic cells. *Science* **318**, 1917–1920 (2007).
6. Kim, J., Koo, B. K. & Knoblich, J. A. Human organoids: model systems for human biology and medicine. *Nat. Rev. Mol. Cell Biol.* https://doi.org/10.1038/s41580-020-0259-3 (2020).
7. Liu, J. et al. Generation and primary characterization of iAM-1, a versatile new line of conditionally immortalized atrial myocytes with preserved cardiomyogenic differentiation capacity. *Cardiovasc. Res.* **114**, 1848–1859 (2018).
8. Liu, J. et al. Conditionally immortalized brown preadipocytes can switch between proliferative and differentiated states. *Biochim. Biophys. Acta Mol. Cell Biol. Lipids* **1864**, 158511 (2019).
9. Deuschle, U., Meyer, W. K. & Thiesen, H. J. Tetracycline-reversible silencing of eukaryotic promoters. *Mol. Cell. Biol.* **15**, 1907–1914 (1995).
10. Szulc, J., Wiznerowicz, M., Sauvain, M. O., Trono, D. & Aebischer, P. A versatile tool for conditional gene expression and knockdown. *Nat. Methods* **3**, 109–116 (2006).
11. Chugh, S. S. et al. Worldwide epidemiology of atrial fibrillation: a Global Burden of Disease 2010 Study. *Circulation* **129**, 837–847 (2014).
12. Kim, M. H., Johnston, S. S., Chu, B. C., Dalal, M. R. & Schulman, K. L. Estimation of total incremental health care costs in patients with atrial fibrillation in the United States. *Circ. Cardiovasc. Qual. Outcomes* **4**, 313–320 (2011).
13. Nattel, S., Heijman, J., Zhou, L. & Dobrev, D. Molecular basis of atrial fibrillation pathophysiology and therapy: a translational perspective. *Circ. Res.* **127**, 51–72 (2020).
14. Heijman, J., Guichard, J. B., Dobrev, D. & Nattel, S. Translational challenges in atrial fibrillation. *Circ. Res.* **122**, 752–773 (2018).
15. Kirchhof, P. The future of atrial fibrillation management: integrated care and stratified therapy. *Lancet* **390**, 1873–1887 (2017).
16. van Gorp, P. R. R., Trines, S. A., Pijnappels, D. A. & de Vries, A. A. F. Multicellular in vitro models of cardiac arrhythmias: focus on atrial fibrillation. *Front. Cardiovasc. Med.* **7**, 43 (2020).
17. Salva, M. Z. et al. Design of tissue-specific regulatory cassettes for high-level rAAV-mediated expression in skeletal and cardiac muscle. *Mol. Ther.* **15**, 320–329 (2007).
18. Huttenbach, Y., Ostrowski, M. L., Thaller, D. & Kim, H. S. Cell proliferation in the growing human heart: MIB-1 immunostaining in preterm and term infants at autopsy. *Cardiovasc. Pathol.* **10**, 119–123 (2001).
19. Cui, Y. et al. Single-cell transcriptome analysis maps the developmental track of the human heart. *Cell Rep.* **26**, 1934–1950.e5 (2019).
20. Consortium, G. T. The genotype-tissue expression (GTEx) project. *Nat. Genet.* **45**, 580–585 (2013).
21. Baker, M. Reproducibility: respect your cells! *Nature* **537**, 433–435 (2016).
22. Narayan, S. M., Shivkumar, K., Krummen, D. E., Miller, J. M. & Rappel, W. J. Panoramic electrophysiological mapping but not electrogram morphology identifies stable sources for human atrial fibrillation: stable atrial fibrillation rotors and focal sources relate poorly to fractionated electrograms. *Circ. Arrhythm. Electrophysiol.* **6**, 58–67 (2013).
23. Balouch, M. et al. Impact of rotor temperospatial stability on acute and one-year atrial fibrillation ablation outcomes. *Clin. Cardiol.* **40**, 383–389 (2017).
24. Laksman, Z. et al. Modeling atrial fibrillation using human embryonic stem cell-derived atrial tissue. *Sci. Rep.* **7**, 5268 (2017).
25. Sanders, P. et al. Spectral analysis identifies sites of high-frequency activity maintaining atrial fibrillation in humans. *Circulation* **112**, 789–797 (2005).
26. Schuessler, R. B. et al. Spatial and temporal stability of the dominant frequency of activation in human atrial fibrillation. *J. Electrocardiol.* **39**, S7–S12 (2006).
27. Yoshida, K. et al. Left atrial pressure and dominant frequency of atrial fibrillation in humans. *Heart Rhythm* **8**, 181–187 (2011).
28. January, C. T. et al. 2014 AHA/ACC/HRS guideline for the management of patients with atrial fibrillation: a report of the American College of Cardiology/American Heart Association Task Force on Practice Guidelines and the Heart Rhythm Society. *J. Am. Coll. Cardiol.* **64**, e1–e76 (2014).
29. Kirchhof, P. et al. 2016 ESC guidelines for the management of atrial fibrillation developed in collaboration with EACTS. *Eur. Heart J.* **37**, 2893–2962 (2016).
30. Hindricks, G. et al. 2020 ESC guidelines for the diagnosis and management of atrial fibrillation developed in collaboration with the European Association of Cardio-Thoracic Surgery (EACTS). *Eur. Heart J.* https://doi.org/10.1093/eurheartj/ehaa612 (2020).
31. Sanguinetti, M. C. & Jurkiewicz, N. K. Two components of cardiac delayed rectifier K+ current. Differential sensitivity to block by class III antiarrhythmic agents. *J. Gen. Physiol.* **96**, 195–215 (1990).
32. Melgari, D., Zhang, Y., El Harchi, A., Dempsey, C. E. & Hancox, J. C. Molecular basis of hERG potassium channel blockade by the class Ic antiarrhythmic flecainide. *J. Mol. Cell. Cardiol.* **86**, 42–53 (2015).
33. Davidson, M. M. et al. Novel cell lines derived from adult human ventricular cardiomyocytes. *J. Mol. Cell. Cardiol.* **39**, 133–147 (2005).
34. Goldman, B. I., Amin, K. M., Kubo, H., Singhal, A. & Wurzel, J. Human myocardial cell lines generated with SV40 temperature-sensitive mutant tsA58. *In Vitro Cell. Dev. Biol. Anim.* **42**, 324–331 (2006).
35. Schwach, V. et al. A COUP-TFII human embryonic stem cell reporter line to identify and select atrial cardiomyocytes. *Stem Cell Rep.* **9**, 1765–1779 (2017).
36. Ban, K., Bae, S. & Yoon, Y. S. Current strategies and challenges for purification of cardiomyocytes derived from human pluripotent stem cells. *Theranostics* **7**, 2067–2077 (2017).
37. Lee, J. H., Protze, S. I., Laksman, Z., Backx, P. H. & Keller, G. M. Human pluripotent stem cell-derived atrial and ventricular cardiomyocytes develop from distinct mesoderm populations. *Cell Stem Cell* **21**, 179–194.e4 (2017).
38. Argenziano, M. et al. Electrophysiologic characterization of calcium handling in human induced pluripotent stem cell-derived atrial cardiomyocytes. *Stem Cell Rep.* **10**, 1867–1878 (2018).

39. Branco, M. A. et al. Transcriptomic analysis of 3D cardiac differentiation of human induced pluripotent stem cells reveals faster cardiomyocyte maturation compared to 2D culture. *Sci. Rep.* **9**, 9229 (2019).
40. Buikema, J. W. et al. Wnt activation and reduced cell-cell contact synergistically induce massive expansion of functional human iPSC-derived cardiomyocytes. *Cell Stem Cell* **27**, 50–63.e5 (2020).
41. Devalla, H. D. et al. Atrial-like cardiomyocytes from human pluripotent stem cells are a robust preclinical model for assessing atrial-selective pharmacology. *EMBO Mol. Med.* **7**, 394–410 (2015).
42. Voigt, N. et al. Enhanced sarcoplasmic reticulum Ca2+ leak and increased Na+-Ca2+ exchanger function underlie delayed afterdepolarizations in patients with chronic atrial fibrillation. *Circulation* **125**, 2059–2070 (2012).
43. Voigt, N. et al. Cellular and molecular mechanisms of atrial arrhythmogenesis in patients with paroxysmal atrial fibrillation. *Circulation* **129**, 145–156 (2014).
44. Heijman, J. et al. Atrial myocyte NLRP3/CaMKII nexus forms a substrate for post-operative atrial fibrillation. *Circ. Res.* https://doi.org/10.1161/CIRCRESAHA.120.316710 (2020).
45. Nakanishi, H. et al. Geometrical patterning and constituent cell heterogeneity facilitate electrical conduction disturbances in a human induced pluripotent stem cell-based platform: an in vitro disease model of atrial arrhythmias. *Front. Physiol.* **10**, 818 (2019).
46. Goldfracht, I. et al. Generating ring-shaped engineered heart tissues from ventricular and atrial human pluripotent stem cell-derived cardiomyocytes. *Nat. Commun.* **11**, 75 (2020).
47. Harrild, D. & Henriquez, C. A computer model of normal conduction in the human atria. *Circ. Res.* **87**, E25–E36 (2000).
48. Valderrabano, M. Influence of anisotropic conduction properties in the propagation of the cardiac action potential. *Prog. Biophys. Mol. Biol.* **94**, 144–168 (2007).
49. Salvage, S. C. et al. Multiple targets for flecainide action: implications for cardiac arrhythmogenesis. *Br. J. Pharmacol.* **175**, 1260–1278 (2018).
50. Lemme, M. et al. Atrial-like engineered heart tissue: an in vitro model of the human atrium. *Stem Cell Rep.* **11**, 1378–1390 (2018).
51. Zhao, Y. et al. A platform for generation of chamber-specific cardiac tissues and disease modeling. *Cell* **176**, 913–927.e18 (2019).
52. Lee, A. et al. 3D bioprinting of collagen to rebuild components of the human heart. *Science* **365**, 482–487 (2019).
53. Yu, H. & Wang, Z. Cardiomyocyte-derived exosomes: biological functions and potential therapeutic implications. *Front. Physiol.* **10**, 1049 (2019).
54. Chang, T. H., Ray, F. A., Thompson, D. A. & Schlegel, R. Disregulation of mitotic checkpoints and regulatory proteins following acute expression of SV40 large T antigen in diploid human cells. *Oncogene* **14**, 2383–2393 (1997).
55. Goette, A. et al. EHRA/HRS/APHRS/SOLAECE expert consensus on atrial cardiomyopathies: definition, characterization, and clinical implication. *Heart Rhythm* **14**, e3–e40 (2017).
56. DuBridge, R. B. et al. Analysis of mutation in human cells by using an Epstein-Barr virus shuttle system. *Mol. Cell. Biol.* **7**, 379–387 (1987).
57. Chen, S., Zhou, Y., Chen, Y. & Gu, J. fastp: an ultra-fast all-in-one FASTQ preprocessor. *Bioinformatics* **34**, i884–i890 (2018).
58. Patro, R., Duggal, G., Love, M. I., Irizarry, R. A. & Kingsford, C. Salmon provides fast and bias-aware quantification of transcript expression. *Nat. Methods* **14**, 417–419 (2017).
59. Love, M. I. et al. Tximeta: reference sequence checksums for provenance identification in RNA-seq. *PLoS Comput. Biol.* **16**, e1007664 (2020).
60. Stuart, T. et al. Comprehensive integration of single-cell data. *Cell* **177**, 1888–1902.e21 (2019).
61. Love, M. I., Huber, W. & Anders, S. Moderated estimation of fold change and dispersion for RNA-seq data with DESeq2. *Genome Biol.* **15**, 550 (2014).
62. Birket, M. J. et al. Contractile defect caused by mutation in MYBPC3 revealed under conditions optimized for human PSC-cardiomyocyte function. *Cell Rep.* **13**, 733–745 (2015).
63. Barry, P. H. & Lynch, J. W. Liquid junction potentials and small cell effects in patch-clamp analysis. *J. Membr. Biol.* **121**, 101–117 (1991).
64. Verkerk, A. O. et al. Patch-clamp recordings of action potentials from human atrial myocytes: optimization through dynamic clamp. *Front. Pharmacol.* **12**, 649414 (2021).
65. Casini, S. et al. Absence of functional Nav1.8 channels in non-diseased atrial and ventricular cardiomyocytes. *Cardiovasc. Drugs Ther.* **33**, 649–660 (2019).
66. van den Berg, N. W. E. et al. PREventive left atrial appenDage resection for the predICtion of fuTure atrial fibrillation: design of the PREDICT AF study. *J. Cardiovasc. Med.* **20**, 752–761 (2019).

Acknowledgements

We thank J. Liu (LUMC, Leiden, the Netherlands) for constructing plasmid pLV.iMHCK7.SV40-LT-WT and producing LV.iMHCK7.SV40-LT-WT particles, T. v. Herwaarden (LUMC, Leiden, the Netherlands) for collecting human foetal atrial tissue, B. Klein (LUMC, Leiden, the Netherlands) for donating the SV40 LT-encoding plasmid pAT153.SV40ori, S. Hauschka (University of Washington, Seattle, WA) for providing the construct +aMHCKChCAT encoding the MHCK7 promoter, D. Trono (Swiss Federal Institute of Technology Lausanne, Lausanne, Switzerland) for making available the LV shuttle plasmid pLVET-tTR-KRAB, C. Jost (LUMC, Leiden, the Netherlands) for assistance with interpretation and annotation of transmission electron microscopy data and U. Ravens (University of Freiburg, Freiburg, Germany) for useful discussions.This publication received financial support from the LUMC Executive Board (PhD fellowship to N.H.) and from the Leiden Regenerative Medicine Platform Holding (LRMPH project 8212/41235 to A.A.F.d.V.). Additional support was provided by the research programme 'More Knowledge with Fewer Animals' (MKMD, project 114022503, to A.A.F.d.V.), which is (partly) financed by the Netherlands Organisation for Health Research and Development (ZonMw) and by the Dutch Society for the Replacement of Animal Testing (dsRAT).

Author contributions

N.H., D.A.P. and A.A.F.d.V. conceived the study, interpreted results and wrote the manuscript. N.H. generated and characterized the hiAM lines with the assistance of S.O.D, J.Z. and L.J.S.L. M.W.V., A.O.V. and M.R.R. performed and analysed patch-clamping experiments. V.S., C.C.F. and R.P. generated hESC-AM layers and assisted with the associated analyses. R.R.S. and G.J.C.V. performed the comparative transcriptome analyses of the different cell types and tissues. A.A.M. generated and interpreted transmission electron microscopy data. W.E.C. performed the flow cytometric ploidy analysis. M.J.T.H.G. provided human foetal atrial material. D.D. assisted in the design and interpretation of the arrhythmia studies. T.J.v.B., R.J.M.K. and M.J.S. provided clinical input to the study. All authors refined the manuscript.

Competing interests

M.J.S., D.A.P. and A.A.F.d.V. are inventors of a patent application (US16/480,280, 'Conditionally immortalized cells and methods for their preparation') related to this work. R.P. is a cofounder of Pluriomics (Ncardia) and River Biomedics. D.D. is a member of the scientific advisory boards of OMEICOS Therapeutics and Acesion Pharma. All other authors declare no competing interests.

Additional information

Supplementary information The online version contains supplementary material available at https://doi.org/10.1038/s41551-021-00827-5.

Correspondence and requests for materials should be addressed to Antoine A. F. de Vries.

Peer review information *Nature Biomedical Engineering* thanks Lior Gepstein and the other, anonymous, reviewer(s) for their contribution to the peer review of this work. Peer reviewer reports are available.